LOAN DOCUMENT

PHOTOGRAPH THIS SHEET

DTIC ACCESSION NUMBER

LEVEL

INVENTORY

D

AFRL-ML-TY-TR-1999-4532

DOCUMENT IDENTIFICATION

30 JAN 98

DISTRIBUTION STATEMENT A
Approved for Public Release
Distribution Unlimited

DISTRIBUTION STATEMENT

HANDLE WITH CARE

ACCESSION FOR

NTIS GRA&I ☒

DTIC TRAC ☐

UNANNOUNCED ☐

JUSTIFICATION

BY

DISTRIBUTION/

AVAILABILITY CODES

DISTRIBUTION	AVAILABILITY AND/OR SPECIAL	
A-1		

DISTRIBUTION STAMP

DATE ACCESSIONED

DATE RETURNED

19990811 081

REGISTERED OR CERTIFIED NUMBER

PHOTOGRAPH THIS SHEET AND RETURN TO DTIC-FDAC

DTIC FORM 70A JUN 90

DOCUMENT PROCESSING SHEET

PREVIOUS EDITIONS MAY BE USED UNTIL STOCK IS EXHAUSTED.

LOAN DOCUMENT

AFRL-ML-TY-TR-1999-4532

USE OF STRONTIUM-LANTHANUM COBALTATE AS A HIGH TEMPERATURE CATALYST FOR NO_X REDUCTION

GERALD P. WIRTZ
MARK A. KELLY

DEPARTMENT OF MATERIALS, SCIENCE AND ENGINEERING
UNIVERSITY OF ILLINOIS AT URBANA-CHAMPAIGN

AIR FORCE RESEARCH LABORATORY
MATERIALS & MANUFACTURING DIRECTORATE
AIRBASE & ENVIRONMENTAL TECHNOLOGY DIVISION
TYNDALL AFB FL 32403-5323

NOTICES

WHEN GOVERNMENT DRAWINGS, SPECIFICATIONS, OR OTHER DATA INCLUDED IN THIS DOCUMENT FOR ANY PURPOSE OTHER THAN GOVERNMENT PROCUREMENT DOES NOT IN ANY WAY OBLIGATE THE US GOVERNMENT. THE FACT THAT THE GOVERNMENT FORMULATED OR SUPPLIED THE DRAWINGS, SPECIFICATIONS, OR OTHER DATA DOES NOT LICENSE THE HOLDER OR ANY OTHER PERSON OR CORPORATION, OR CONVEY ANY RIGHTS OR PERMISSION TO MANUFACTURE, USE, OR SELL ANY PATENTED INVENTION THAT MAY RELATE TO THEM.

THIS REPORT IS RELEASABLE TO THE NATIONAL TECHNICAL INFORMATION SERVICE (NTIS). AT NTIS, IT WILL BE AVAILABLE TO THE GENERAL PUBLIC, INCLUDING FOREIGN NATIONS.

THIS TECHNICAL REPORT HAS BEEN REVIEWED AND IS APPROVED FOR PUBLICATION.

JOSEPH D. WANDER, PhD
Project Manager

CHRISTINE WAGENER-HULME, Lt Col, USAF, BSC
Chief, Environmental Technology Development Branch

ANDREW D. POULIS
Scientific & Technical
Information Program Manager

for **RANDY L. GROSS, Lt Col, USAF, BSC**
Chief, Airbase & Environmental
Technology Division

IF YOUR ADDRESS HAS CHANGED, IF YOU WISH TO BE REMOVED FROM OUR MAILING LIST, OR IF THE ADDRESSEE IS NO LONGER EMPLOYED BY YOUR ORGANIZATION, PLEASE NOTIFY AFRL/MLQP, TYNDALL AFB, FLORIDA 32403-5323, TO HELP MAINTAIN A CURRENT MAILING LIST.

Do not return copies of this report unless contractual obligations or notice on a specific document requires its return.

REPORT DOCUMENTATION PAGE

Form Approved
OMB No. 0704-0188

1. AGENCY USE ONLY *(Leave blank)*	2. REPORT DATE	3. REPORT TYPE AND DATES COVERED
	January 30, 1998	Final 1997 to January 1998

4. TITLE AND SUBTITLE
Use of Strontium-Lanthanum Cobaltate as a High Temperature Catalyst for NOx Reduction

5. FUNDING NUMBERS
Contract Purchase Order
DACA88-93-D-0018-24
Purchase Request No.
W52EU2-5207-9620

6. AUTHOR(S)
Wirtz, Gerald P., and Kelly, Mark A.

7. PERFORMING ORGANIZATION NAME(S) AND ADDRESS(ES)
Department of Materials Science and Engineering
University of Illinois at Urbana-Champaign

8. PERFORMING ORGANIZATION REPORT NUMBER

9. SPONSORING/MONITORING AGENCY NAME(S) AND ADDRESS(ES)
Monitor: U.S. Army Construction Engineering Research Laboratories
Sponsor:
Air Force Research Laboratory (AFRL/MLQE)
139 Barnes Dr. Ste 2
Tyndall AFB, FL 32403

10. SPONSORING/MONITORING AGENCY REPORT NUMBER
AFRL-ML-TY-TR-1999-4532

11. SUPPLEMENTARY NOTES
Sponsor Tech POC is Dr. Joe Wander, AFRL/MLQE, (850) 283-6240

12a. DISTRIBUTION AVAILABILITY STATEMENT
Approved for Public Release: Distribution Unlimited

(PA Case File#ASC-99-1627)

12b. DISTRIBUTION CODE
A

13. ABSTRACT *(Maximum 200 words)*

The primary objective of this work was to assess whether Strontium-Lanthanum Cobaltate shows promise as a high temperature catalyst for NOx reduction as an initial step in a program to develop useful NOx catalysts. The determination of the thermodynamic and kinetic stability of the active oxygen deficient phases in NOx atmospheres and the initial evaluation of the effectiveness of the catalyst for NOx reduction were secondary objectives to be included in this assessment.
From XRD, DTA and simultaneous TGA/DSC measurements the A-site deficient composition was found to be chemically and structurally stable over a wide range of temperatures in air and simulated exhausts. This material will catalyze the reduction of NO to N2 in the presence of CO under fuel-lean, stoichiometric and fuel rich conditions, and is particularly effective at low temperature. Combining substrate materials which seem to enhance NO reduction at high temperatures with the perovskite catalyst, which works best at lower temperatures, holds promise as a synergistic emission control system.

14. SUBJECT TERMS	15. NUMBER OF PAGES
NOX, Strontium-Lanthanum Cobaltate, NOx Catalyst	
	16. PRICE CODE

17. SECURITY CLASSIFICATION OF REPORT	18. SECURITY CLASSIFICATION OF THIS PAGE	19. SECURITY CLASSIFICATION OF ABSTRACT	20. LIMITATION OF ABSTRACT
UNCLASSIFIED	UNCLASSIFIED	UNCLASSIFIED	UNL

CLASSIFIED BY:

DECLASSIFY ON:

Executive Summary

The primary objective of this work was to assess whether $Sr_xLa_{1-x}CoO_3$ shows promise as a high temperature catalyst for NO_x reduction as an initial step in a program to develop useful NO_x catalysts. The determination of the thermodynamic and kinetic stability of the active oxygen deficient phases in NO_x atmospheres and the initial evaluation of the effectiveness of the catalyst for NO_x reduction were secondary objectives to be included in this assessment. Another objective of this effort was to assemble a facility to conduct ongoing research on the use of rare earth perovskite-type oxides as NO_x abatement catalysts.

Catalyst material was prepared by typical ceramic methods involving mixing of dry powders of the desired composition, wet milling of these reagents for 2 hours in alcohol, calcination at 1000°C for about 10 hours, followed by remitting and repetition of the calcination. The desired attributes of the final powder included: (a) fine particle size (<10, μm) to promote the catalytic activity of the material, and (b) complete reaction of the starting materials to form single phase perovskite-type compounds of the designed composition.

While the literature indicates that strontium doped lanthanum cobaltates will act as low–temperature catalysts for NO reduction, it is not obvious that they would be stable at high temperatures. Two bench scale reactors for the evaluation of high temperature catalytic properties of the prepared cobaltate material were designed and constructed. The reactors were designed to test the catalyst in different gas mixtures, simulating combustion exhaust gas streams.

From XRD, DTA and simultaneous TGA/DSC measurements the A-site deficient composition $(La_{0.7}Sr_{0.3})_{0.9}CoO_{2.715}$ was found to be chemically and structurally stable over a wide range of temperatures in air and simulated exhausts. This material will catalyze the reduction of NO to N_2 in the presence of CO under fuel-lean, stoichiometric and fuel rich conditions, and is particularly effective at low temperature. However, the design of any system to do this will be critical because it appears that the kinetic limitations of the reactions would obviate the need for increased contact time between the reactant gases and the catalyst, especially in the lower temperature regime. In addition, the zirconia and alumina materials from which the reactor was constructed definitely appear to enhance the reduction of nitric oxide to nitrogen in the presence of carbon monoxide. Combining substrate materials which seem to enhance NO reduction at high temperatures with the perovskite catalyst, which works best at lower temperatures, holds promise as a synergistic emission control system.

TABLE OF CONTENTS

LIST OF FIGURES

LIST OF TABLES

Use of Strontium-Lanthanum Cobaltate as a High Temperature Catalyst for NOx Reduction

Final Report

Objective

The primary objective of this work was to assess whether $Sr_xLa_{1-x}CoO_3$ shows promise as a high temperature catalyst for NO_x reduction as an initial step in a program to develop useful NO_x catalysts. The determination of the thermodynamic and kinetic stability of the active oxygen deficient phases in NO_x atmospheres and the initial evaluation of the effectiveness of the catalyst for NO_x reduction were secondary objectives to be included in this assessment. Another objective of this effort was to assemble a facility to conduct ongoing research on the use of rare earth perovskite-type oxides as NO_x abatement catalysts.

Background

Strontium doped lanthanum cobaltate, $Sr_xLa_{1-x}CoO_3$, was first suggested in 1971 as a catalyst for automotive exhaust pollution control by Libby,[1] based on the report of Meadowcroft[2] that $Sr_xLa_{1-x}CoO_3$ rivaled platinum as an oxygen electrode in high temperature electrochemical cells. Based on the Libby suggestion, Sorenson *et al.*[3] studied $LaCoO_3$ as a catalyst in engine exhaust gases and discovered that above 650°C it seemed to be effective for NO_x reduction as well as CO and hydrocarbon oxidation. An early review of the properties of perovskite compounds as nitric oxide catalysts was provided by Voorhoeve *et al.*[4] in 1977. That same year, a more comprehensive review of the catalytic properties of perovskites and related compounds was published[5] by the same group at Bell Laboratories. Since that time, a large number of papers have been published on rare earth perovskites as catalysts for the reduction of nitrogen oxides, of which a few might be cited.[6–10] A recent book, edited by Tejuca and Fierro, contains several contributed chapters by the most prominent workers in the field on the catalytic properties and applications of perovskite type oxides.[11]

There is an equally broad literature of the rare earth perovskites in electrocatalytic applications as electrodes on high temperature solid oxide fuel cells and other high temperature electrochemical cells. The use of the perovskites of formula $LaMO_3$ (M = Co, Mn, Fe, Cr) as air electrodes for high temperature fuel cells was first proposed by Tedmon *et al.*[12] Whether the application is catalytic or electrocatalytic, it is generally accepted that the adsorption of reactants is the first step in the process, and that this step involves electronic exchange between the adsorbate and substrate.[13,14] The most commonly assumed adsorption sites in perovskites-type oxides are oxygen vacancies.[15,16] In an electrochemical cell, the electrocatalytic reaction rate on the electrode will be represented by the cell current, which will be given by:[17,18]

$$I = 2FS^2\overline{P_{O_2}}\left(1-\bar{e}\right)^2\frac{\left[\exp\left(\frac{4F\varsigma}{RT}\right)-1\right]}{\left\{1-\bar{e}\left[1-\exp\left(\frac{2F\varsigma}{RT}\right)\right]\right\}^2}$$

assuming a Langmuir adsorption isotherm, where $\overline{P_{O_2}}$ is the ambient oxygen partial pressure and $\bar{\theta}$ is the zero current fraction of surface sites covered by reactant. The catalytic activity of the electrode is represented by the product kS^2 where S is the surface concentration of adsorption sites and k is the rate constant representing the activity of the individual adsorption sites. The catalytic activity of the surface is therefore related to the defect chemistry of the oxide via the term S. which represents the surface concentration of oxygen vacancies, and the catalytic activity of these sites via the term k, which varies from one material to the next and is subject to modification by doping the oxide.[19]

Of the $LaMO_3$ materials (M = Mn, Co, Fe, Cr), $LaCoO_3$ appears to give the best catalytic activity for the reduction of nitrogen oxides,[20] presumably because of the greater activity of the individual oxygen vacancy sites. In the pure state the concentration of these oxygen vacancies will vary with the oxygen potential at the surface, which in turn may vary with the degree of coverage by the reactant. During the conversion process, the cobaltate catalyst may be reduced through a complex series of reactions, which can eventually result in structural changes, and loss of catalytic activity. The replacement of some La by Sr ions results in strontium-doped lanthanum cobaltate, normally designated $Sr_xLa_{1-y}CoO_3$. In fact, the replacement of La by Sr would be accomplished by the following chemical reaction:

$$ySrO + yCoO + (1-y)LaCoO_3 + \frac{y}{4}O_2 \rightarrow Sr_yLa_{1-y}CoO_{3-\frac{y}{2}}$$

which emphasizes the fact that y/2 oxygen vacancies per formula unit are produced by the substitution if the original valence of the cations is retained. This concentration is much higher than the intrinsic concentration in the pure cobaltate and chemically fixes the concentration of oxygen vacancies, thereby increasing significantly the concentration of adsorption sites on the catalyst surface. It also seems to structurally stabilize the material, decreasing its sensitivity to variations in the ambient atmosphere.

In the terminology of perovskite crystal chemistry, the La cation site is called the A-site, and the Co site is called the B-site. Sr is an A-site cation substitution. It has been further reported that a net A-site cation deficiency further stabilizes the structure, particularly in terms of high temperature reactions with stabilized zirconia substrates in high temperature fuel cell applications.[21] Since it is envisioned that the ultimate application of this material in the present study may be as a thin coating on a stabilized zirconia heat barrier in an advanced jet engine, this compositional aspect of the material is also being pursued. The batching formula for the resultant composition is:

$$(1-x)ySrO + (x+y-xy)CoO + (1-y)(1-x)LaCoO_3 + \frac{1}{4}(x+y-xy)O_2 \rightarrow (Sr_yLa_{(1-y)})_{1-x}CoO_{3-\frac{3}{2}x-\frac{1}{2}y(1-x)}$$

which also indicates that the oxygen ion vacancy concentration will be further enhanced by the A-site cation deficiency.

General Statement of the Work

The proposed work was broken down into a number of tasks, which form the headings of this section of the report.

1. Materials Acquisition/Preparation

Catalyst material was prepared by typical ceramic methods involving mixing of dry powders of the desired composition, wet milling of these reagents for 2 hours in alcohol, calcination at 1000°C for about 10 hours, followed by remitting and repetition of the calcination. The starting raw materials were high purity grade La_2O_3, $SrCO_3$ and CO_3O_4 (or $CoCO_3$). Pure $LaCoO_3$, as well as strontium doped $LaCoO_3$ were prepared and studied by x-ray diffraction to determine the degree of reaction and resultant phases present. Based on these results, electrocatalytic properties, thermal stability and low reactivity discussed in the previous section, the composition

$$(Sr_yLa_{(1-y)})_{1-x}CoO_{3-\frac{3}{2}x-\frac{1}{2}y(1-x)}$$

with x=0.1 and y=0.3 was identified as holding the greatest promise for the present application. Because future plans called for the plasma-spray deposition of this material on YSZ substrates, another coarser (+200 mesh, >74μm) batch of powder was prepared by dry mixing the precursors (eliminating the wet milling steps) and calcining, followed by sieving.

The desired attributes of the final powder included: (a) fine particle size (<10, μm) to promote the catalytic activity of the material, and (b) complete reaction of the starting materials to form single phase perovskite-type compounds of the designed composition. Particle size was measured by sedimentation rate, and Figure 1 shows the raw Sedigraph plot of cumulative mass percent vs. equivalent spherical diameter for the wet and dry milled powders. The average particle size of the wet milled powder is seen to be about 3.5 μm, while that of the dry milled powder is 17 μm. Figure 2 shows the powder x-ray diffraction pattern for the -200 mesh (<74 μm) wet milled material using Cu Kα radiation. The pattern is essentially that of a single phase primitive cubic structure, as expected for lanthanum cobaltate stabilized with strontium. The pattern was indexed and each peak in Figure 2 is labeled with the cubic Miller indices of the planes diffracting. The cubic lattice parameter is approximately 3.84Å. The 220 line at 69.4° 2θ shows evidence of splitting into a doublet, which is indicative of a possible rhombohedral distortion of the lattice, but is not indicative of a second phase. There is evidence of a weak peak at 42.3°, which is likely evidence of remnants of one of the precursor phases. The interplanar spacings and corresponding Miller indices for the as-prepared fine cobaltate powder are listed in Table 1, along with the Miller indices of the possible rhombohedral and hexagonal planes into which the cubic diffraction peaks could split. Pure $LaCoO_3$ has been reported to have a rhombohedral distortion of a cubic lattice. For practical purposes the material is seen to be single-phase cubic perovskite. One (1) kilogram of this material was prepared.

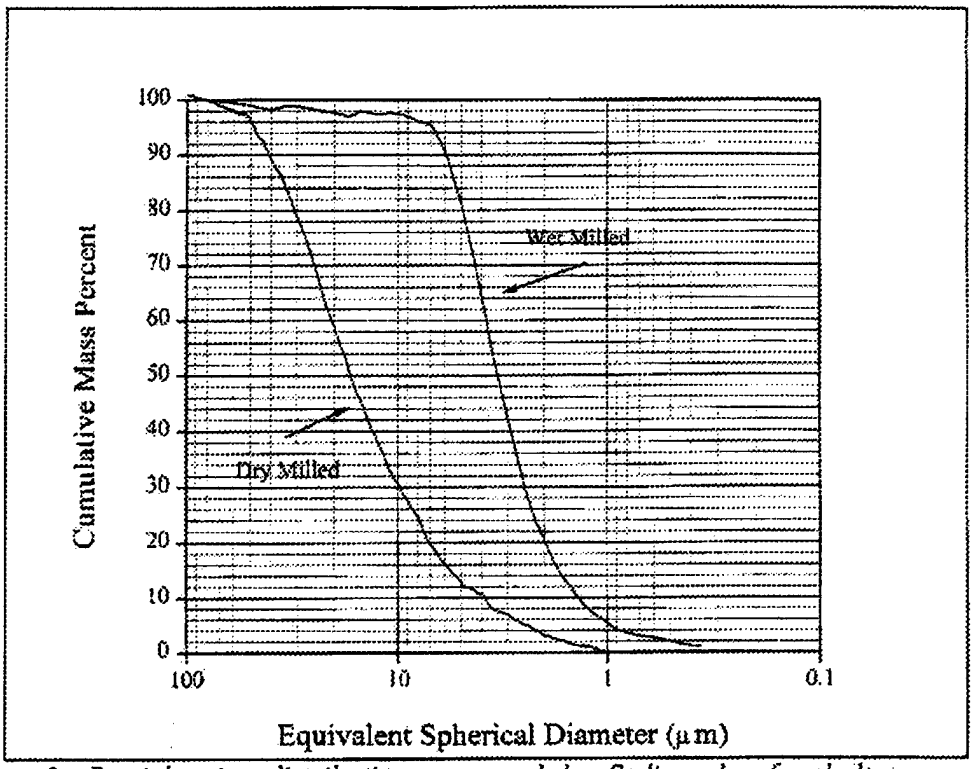

Figure 1: Particle size distribution measured by Sedigraph of cobaltate powders prepared by repeated wet or dry milling and calcination at 1000°C.

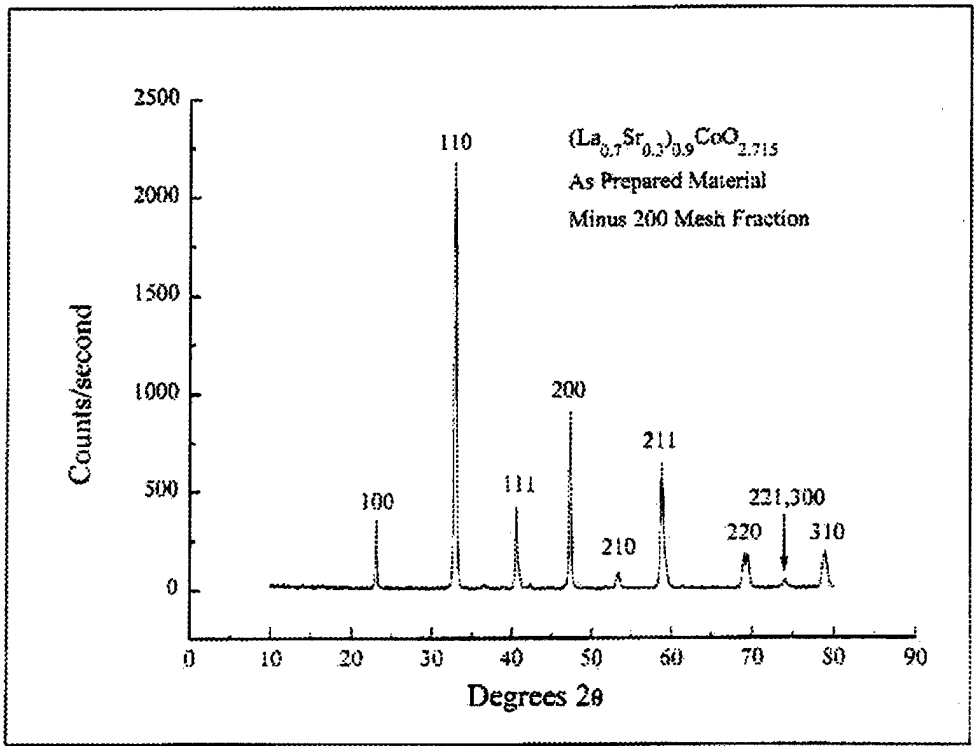

Figure 2: XRD pattern of $(Sr_{0.3}La_{0.7})_{0.9}CoO_{2.715}$ calcined powder, showing the formation of the pure perovskite phase.

Table 1: Interplanar spacings and Miller indices assigned to the listed diffraction angles for the fine cobaltate powder.

2θ	d (Å)	Hkl (cubic)	Hkl (rhombohedral)	Hkl (hexagonal)
23.0	3.86672	100	110	12
33.0	3.838586	110	211; $1\bar{1}0$	110;104
40.6	3.848662	111	222; 002	202;006
47.4	3.835822	200	220	24
53.4	3.836439	210	312; $1\bar{1}2$	122;116
59.0	3.83473	211	323; $11\bar{2}$; 103	030;214;018
69.3	3.835	220	422, $2\bar{2}0$	220;208
74.1	3.838431	221;300	433;$03\bar{1}$;411;330	312;306;1010
79.0	3.832547	310	413;$32\bar{1}$	134;128

2. High Temperature Phase Stability

While the literature indicates that strontium doped lanthanum cobaltates will act as low–temperature catalysts for NO reduction, it is not obvious that they would be stable at high temperatures. Thermogravimetric analysis (TGA), differential thermal analysis (DTA), differential scanning calorimetry (DSC), and powder x-ray diffraction were used to determine the thermal and compositional stability of the prepared catalyst materials in air and in combustion exhaust gases. It is possible to replace up to 30% of the Co with Mn or Fe, with the expectation that the chemical and structural stability of the catalyst would be improved, although the catalytic activity would be degraded.

a) Test at 1220°C

TGA/DSC analyses were performed on the A-site deficient lanthanum cobaltate material characterized as previously detailed, with heating and cooling rates of 10°C/min and a high temperature hold at 1220°C for 10 hours in a typical, simulated exhaust gas mixture. Containing approximately 10% CO_2, 5% 0_2, 2% H_2O, and 0.5% NO_2 in a balance of N_2, the simulated exhaust gas was prepared by mixing gases of composition 10 vol. % CO in CO_2, and 10.5 vol. % NO_X in N_2. The water vapor concentration in the simulated atmosphere was introduced as "wet" air by passing air through water before entering the furnace. Figure 3 shows the results of simultaneous TG and DSC measurements as a function of temperature for the heating and cooling segments of the run. The lower two curves represent the thermogravimetric analysis and the upper curves the differential scanning calorimetric analysis. Figure 4 shows the results of simultaneous TG (lower curve) and DSC (upper curve) measurements as a function of time during the 10 hour hold at 1220°C.

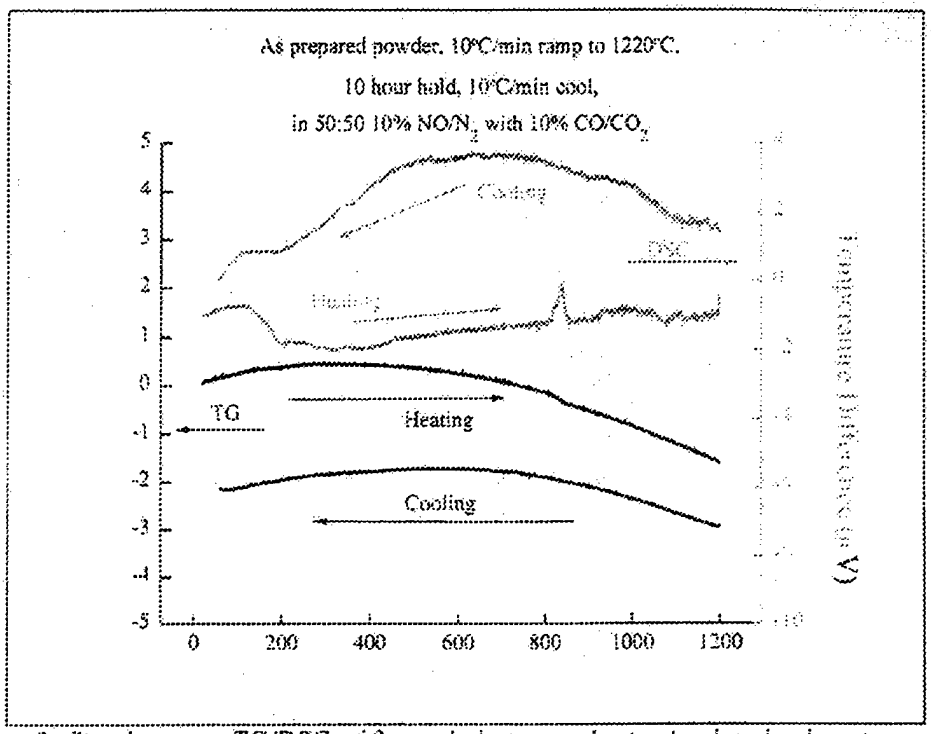

Figure 3: Simultaneous TG/DSC of fine cobaltate powder in simulated exhaust stream to 1220°C. Heating and cooling rates of 10°C/min, with 10 hour dwell at 1220°C.

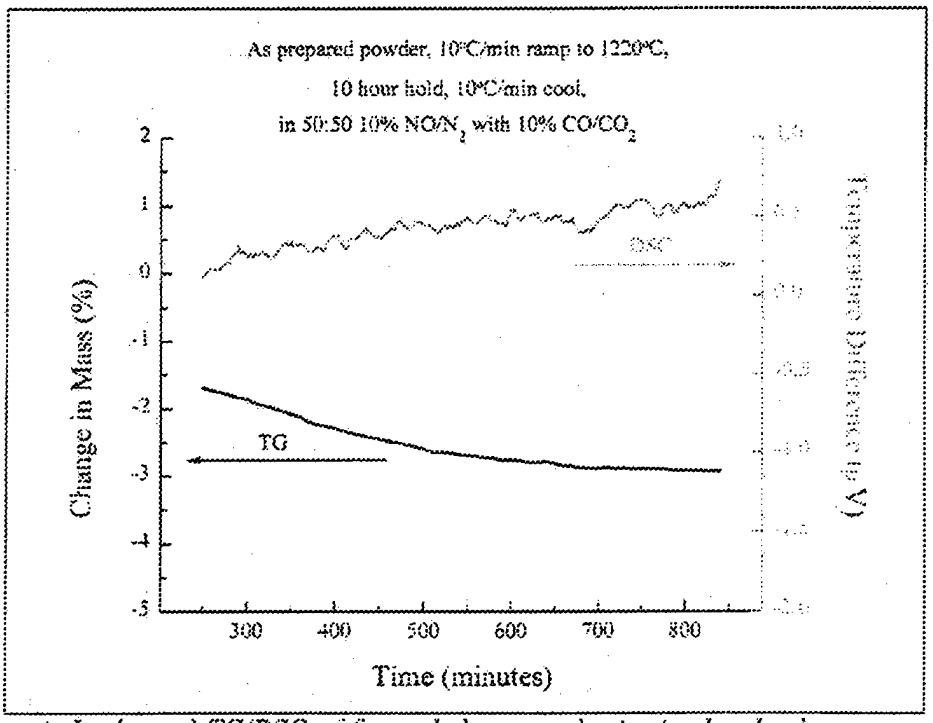

Figure 4: Isothermal TG/DSC of fine cobaltate powder in simulated exhaust stream to 1220°C. Heating and cooling rates of 10°C/min, with 10 hour dwell at 1220°C.

Differential scanning calorimetry showed a single small endothermic peak at 820°C in Figure 3 coincident with a slight, but sudden weight loss in the corresponding TG curve. This was almost certainly associated with the decomposition of remaining unreacted starting materials (probably carbonate). The final weight after cooling was about 1.85% less than the starting weight, as seen in Figure 3. Most of the weight loss occurred during the dwell at maximum temperature. The small continuous endothermic trend during heating and cooling is probably related more to the difference in thermal capacity of the sample and standard than to any real reaction of the material.

Figure 4 shows the monotonic weight loss with time at 1220°C. The total isothermal weight loss was about 1.25%. The corresponding DSC curve shows that during the dwell at 1200°C any thermal evolution was practically undetectable. If the weight loss corresponds to reduction of the sample, and at some degree of reduction the perovskite structure decomposed into some reduced phase(s), a corresponding endothermic peak would have been expected in the DSC curve. This is seen as evidence that the perovskite has a high degree of structural stability in this simulated exhaust environment.

Assuming that the total weight loss can be ascribed to the creation of oxygen vacancies, it is possible to estimate the number of additional oxygen vacancies formed. A total weight loss of 1.25% would correspond to a vacancy creation of 0.17 per formula unit of $(La_{0.7}Sr_{0.3})_{0.9}CoO_3$. Assuming the nominal valence states of the cations (La^{3+}, Sr^{2+} and Co^{3+}) and a perfect Co ion sublattice, the starting material would have a vacancy concentration of 0.285 per formula unit, or a composition of $(La_{0,7}Sr_{0,3})_{0.9}CoO_3$. Adding the additional oxygen vacancies formed at 1200°C in the simulated exhaust gas, the final oxygen-deficient composition at 1200°C would be calculated to be $(La_{0,7}Sr_{0,3})_{0.9}CoO_{2.545}$. This would correspond to 15% of the oxygen sites being vacant, which does not seem unreasonable. The minimum decomposition reaction for the perovskite would take the form:[11]

$$4LaCoO_3 \rightarrow La_4Co_3O_{10} + CoO + \frac{1}{2}O_2$$

which, based on the composition $(La_{0,7}Sr_{0,3})_{0.9}CoO_{2.715}$ would correspond to a weight loss of >1.9%, depending on the assumption made about the vacancy concentration in the sub-oxide formed.

For comparison, Mizusaki *et al.*[22] determined total oxygen vacancy concentrations of about 4.3% at 800°C and $P_{O_2} = 10^{-4}$ atm, for $La_{0,7}Sr_{0,3}CoO_{3-z}$. This value increased to 5% at 850°C for similar P_{O_2} values. Nakamura *et al.*[23] estimated initial decomposition oxygen pressures between 10^{-7}-10^{-5} atm at 850-1000°C for the unsubstituted perovskite $LaCoO_3$, with initial formation of La_2CoO_4 + CoO, further decomposing to $La_2O_3 + Co + \frac{1}{2}O_2$, when the oxygen partial pressure dropped to 10^{-13} atm. It seems likely that the actual decomposition path would involve the initial formation of $La_4Co_3O_{10}$+CoO as stated above, based on phase equilibria studies in the system.[11] The fact that all of these structures are closely related to the perovskite structure makes their identification by powder x-ray diffraction problematic. That the decomposition reaction at 820°C is not due to the formation of $La_4Co_3O_{10}$ is concluded from the

fact that this reaction would produce a weight change of 2% and the observed weight change at 820°C was < 0.2%.

The total weight change seems suggestive, but the decomposition to $La_4Co_3O_{10}$ would not occur so continuously over such a broad temperature range.[13]

The initial DSC results of this study are therefore interpreted to mean that decomposition did not occur, which supports the hypothesis that the A-site deficient perovskite is actually more stable than the A-site stoichiometric composition.

Powder XRD analyses of the as prepared material subjected to various heat treatments in air were performed to confirm the stability of the perovskite structure and further check for the presence of new phases. Figure 5 shows the diffraction pattern after the fine cobaltate powder was annealed at 1300°C for 8 hours and slowly cooled to room temperature. It is closely related to the pattern of Figure 2, but differs in that the diffraction peaks are split into multiplets, indicating a slight distortion of the cubic structure to a structure of lower symmetry.

Figure 6 is the diffraction trace for the coarse cobaltate powder after it was subjected to the same annealing cycle as the fine powder. The presence of many peaks which have tentatively been determined to belong to the cobalt, deficient phase $(SrLa)_2CoO_4$ and possibly $(SrLa)_4Co_3O_{10}$, along with the possibility of unreacted or exsolved cobalt oxides, is most probably due to incomplete reaction of the starting materials. Again the perovskite peaks were resolved into multiplets.

To determine if phases which had formed at high temperatures could be recombined at lower temperatures, both fine and coarse cobaltate powders were annealed in air at 1300°C for 8 hours, fast cooled (~50°C/min) to 900°C, annealed again for 20 hours, and slow cooled to room temperature. If oxygen loss at high temperatures was responsible for weight loss, resulting in the formation of cobalt oxide and cobalt-deficient–cobaltate phases, the lower-temperature anneal might provide sufficient thermal energy for them to recombine. Figure 7 shows the results of diffraction analysis for the fine cobaltate powder. No significant differences were found between this trace and the one in Figure 5 for the powder annealed at 1300°C and slowly cooled. The weak peak near 42° 2θ was slightly enhanced for the powder sample subjected to the two–step anneal, but the material was still essentially all perovskite, although distorted from the cubic structure. X-ray diffraction did not show any significant difference between the doubly annealed coarse powder and the coarse powder annealed only at 1300°C. All of the peaks found in Figure 6, the results for the singly annealed coarse powder, are also found in Figure 8, the diffraction trace for the doubly annealed sample.

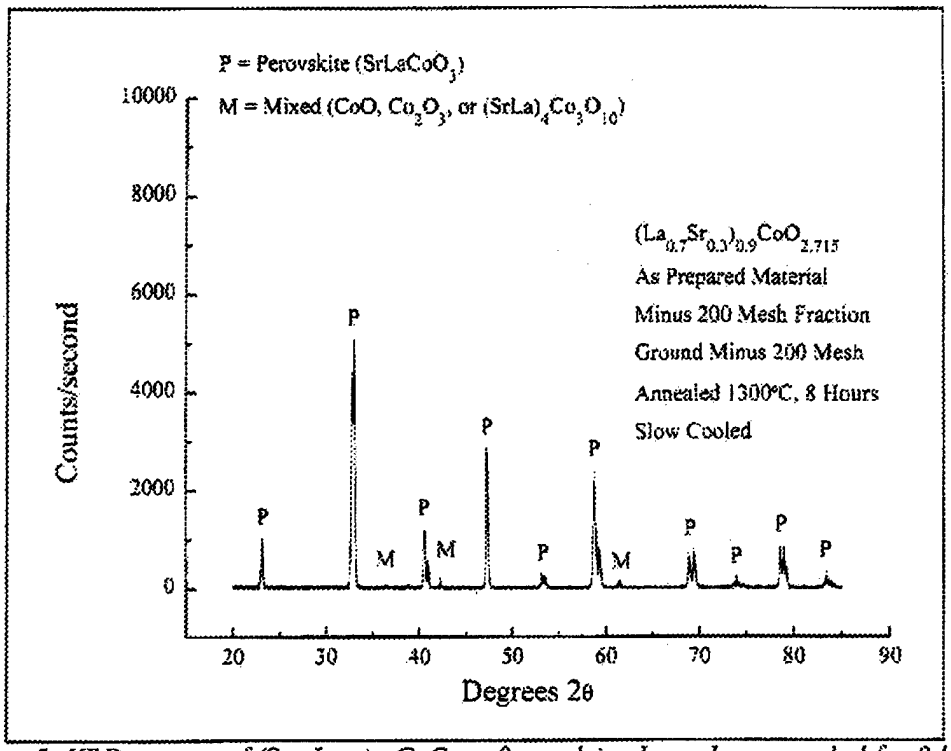

Figure 5: XRD pattern of $(Sr_{0.3}La_{0.7})_{0.9}CoO_{2.715}$ fine calcined powder, annealed for 8 hours at 1300°C and slow cooled to room temperature.

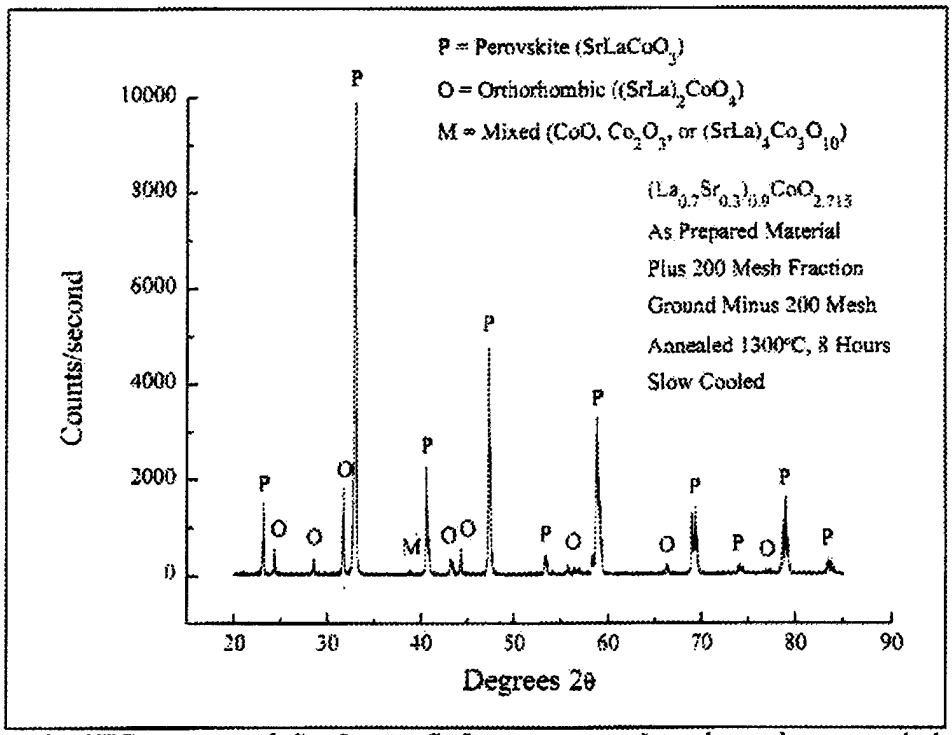

Figure 6 : XRD pattern of $(Sr_{0.3}La_{0.7})_{0.9}CoO_{2.715}$ coarse calcined powder, annealed for 8 hours at 1300°C and slow cooled to room temperature.

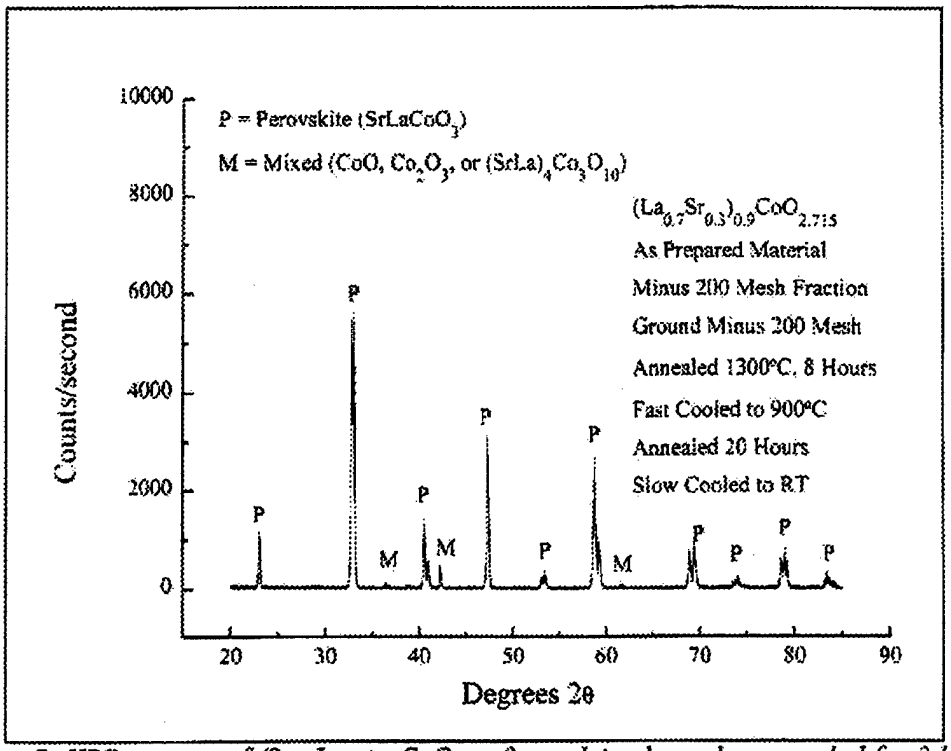

Figure 7: XRD pattern of $(Sr_{0.3}La_{0.7})_{0.9}CoO_{2.715}$ fine calcined powder annealed for 8 hours at 1300°C, fast cooled to 900°C, and slow cooled to room temperature.

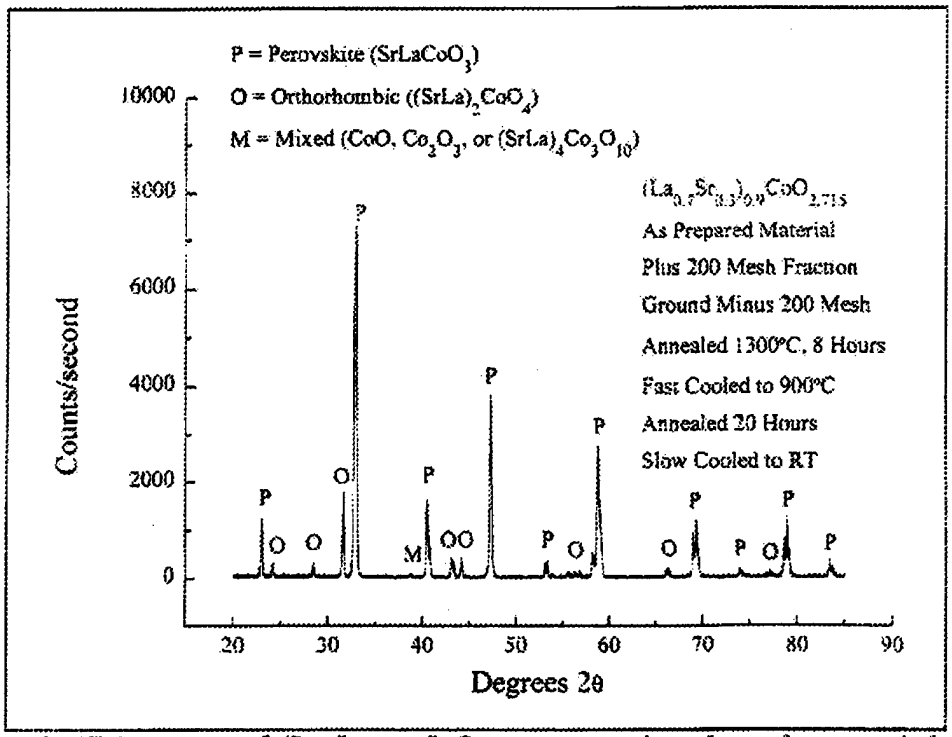

Figure 8: XRD pattern of $(Sr_{0.3}La_{0.7})_{0.9}CoO_{2.715}$ coarse calcined powder annealed for 8 hours at 1300°C, fast cooled to 900°C, and slow cooled to room temperature.

b) Test at 1420°C

The simultaneous TGA/DSC test was repeated on a fresh powder sample using a similar heat/dwell/cool cycle, except that the maximum temperature and the dwell temperature was raised to 1420°C to: (a) confirm the previous analyses, and (b) check the stability at higher temperatures. Heating and cooling results are shown in Figure 9.

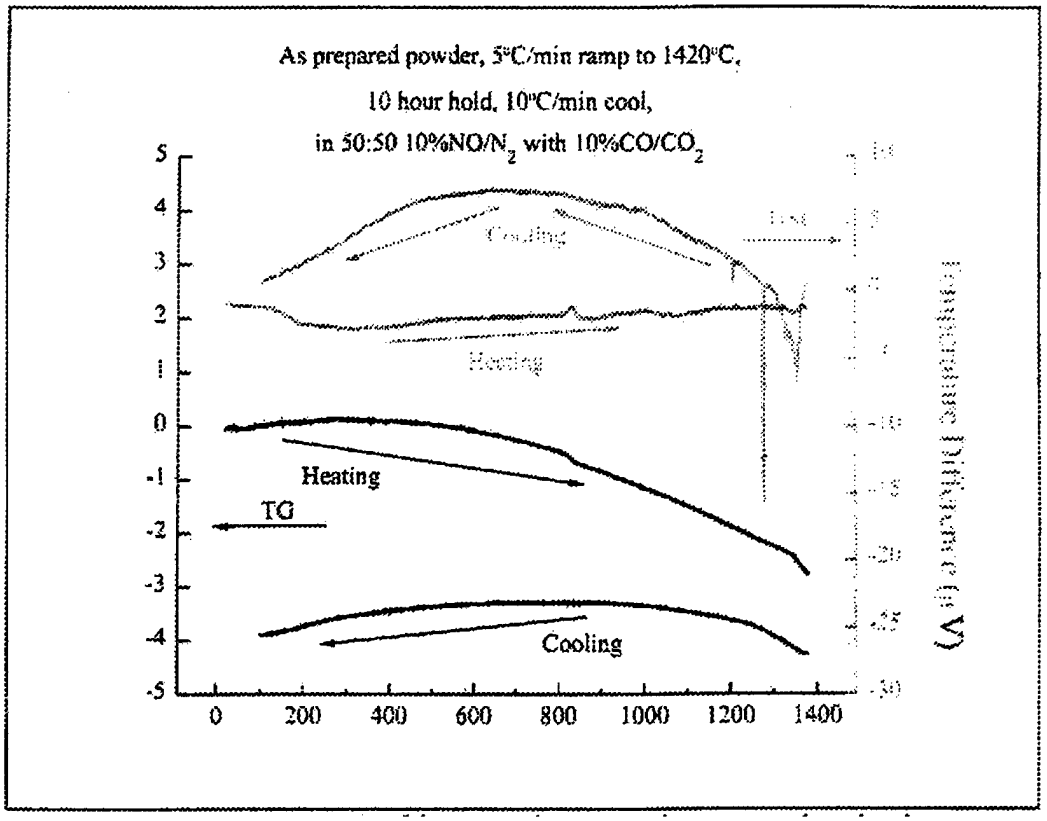

Figure 9: Simultaneous TG/DSC of fine cobaltate powder in simulated exhaust stream to 1420°C. Heating at 5°C/min, cooling at 10°C/min, with 10-hour dwell at 1420°C.

In Figure 9, the general behavior is seen to be very reproducible up to 1200°C in both the TGA and DSC analyses, with a total weight loss in the vicinity of 2% and an endothermic peak with associated weight loss observed at about 820°C. This peak is again thought to be due to the decomposition of residual carbonate. Above 1200°C the rate of weight loss remains more or less constant with increasing temperature up to about 1350°C. At 1350°C another endothermic peak is visible in the DSC curve. A sudden increase in the rate of weight loss is also observed at 1350°C in the simultaneous TGA curve. This reaction has been tentatively ascribed to melting of the perovskite, based on the appearance of the sample after cool down. Confounding this conclusion is the fact that strontium reacts strongly with platinum, the material of which the DSC sample crucibles were made.

The DSC cooling curve shows three exothermic peaks from the peak temperature to 1200°C. Weight gain on cooling from 1420-1200°C is also relatively rapid, indicating that oxidation is an important component of the chemical processes represented by the exothermic peaks observed. It is proposed that the initial broad exotherm corresponds to solidification, and

the two subsequent sharper exotherms represent structural change occurring when the oxidation level reaches some fixed value. Below the final exotherm at 1200°C the material is thought to be equivalent to the starting perovskite. From these TGA/DSC results it can be concluded that the A-site deficient perovskite is structurally and compositionally stable up to 1350°C in this simulated exhaust atmosphere. This is seen as encouraging for the prospects of using this material as a NO_X catalyst in jet engine exhaust.

Nothing significant seems to be occurring during the dwell step at 1420°C as seen in Figure 10. There is a slight additional weight loss, reaching nearly 3% total. Most of the weight loss occurs in the first half of the dwell period, indicating that some equilibrium level was reached. Again, it seems reasonable to conclude that before melting the perovskite structure is stable, with no noticeable decompositional reactions observed by DSC.

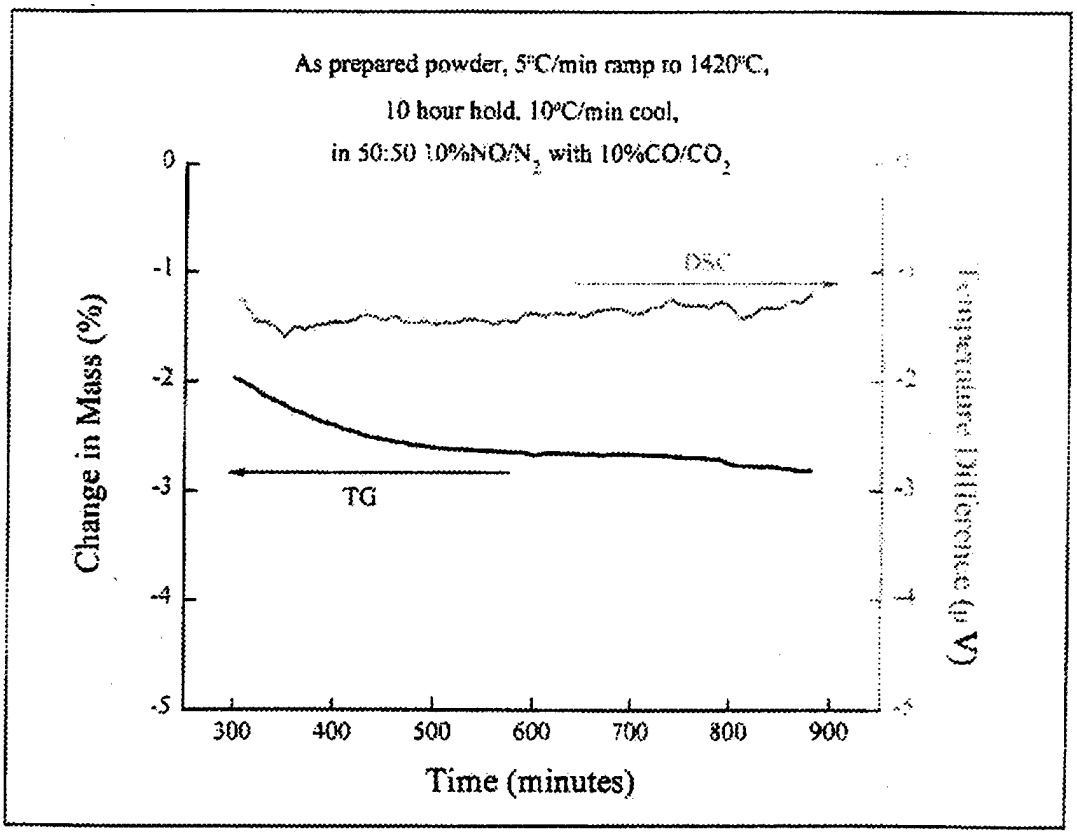

Figure 10: Isothermal TG/DSC of cobaltate powder in simulated exhaust stream during 10-hour dwell at 1420°C.

c) Plasma-arc Sprayed Powders

The application of a coating of $(Sr_{0.3}La_{0.3})_{0.9}CoO_{2.715}$, or any other composition in this class of perovskites, to a solid electrolyte substrate, such as yttria-stabilized zirconia (YSZ), is a key issue in the development of a workable catalyst system. Plasma spraying is an effective technique for developing intimate contact between the perovskite and electrolyte.

Because plasma-arc spraying is the application method of choice, an investigation into the stability of the cobaltate powder in the plasma-arc spraying process was carried out. Upon

the recommendation of the plasma-arc spray unit manufacturer, the fine cobaltate powder was chosen for these tests, and for subsequent tests. Using the recommended power settings, approximately 100 g of powder was applied to a flat, partially stabilized zirconia substrate. By applying material over already coated areas, large amounts of monolithic coating were effectively spelled from the substrate. This material was ground finer than 200 mesh (<74, μm) and analyzed by XRD.

The results of that analysis are shown in Figure 11, and they indicate that high-temperature, cobalt–deficient phases are quenched. Then the presumably molten material is splat cooled on the substrate in the plasma-arc spraying process.

The fine cobaltate powder was also plasma-arc sprayed on a YSZ tube, but only a thin (~50μm) coating was applied. The as-sprayed surface was examined in a scanning electron microscope. Figure 12, a secondary electron image at a magnification of 950X, clearly shows that the material was molten when it impacted the surface. Cooling was very rapid, as there was no apparent rearrangement of the surface structure from the original splat-cooled morphology.

Since the plasma-arc spraying process cools the applied material so quickly when it impacts the substrate, the phases produced are often not at equilibrium. To test this for the cobaltate powder, we annealed, a sample of the crushed plasma–arc sprayed material at 1300°C for 8 hours and slowly cooled it to room temperature. The results of the XRD performed on this material are shown in Figure 13. Most notable about these data when compared to those in Figure 11 is the sharpness of the diffraction peaks. Also of note is the permanence of the cobalt-deficient phases. These data indicate the need to manipulate the chemistry of the powders before they are sprayed to ensure that the final coating is pure perovskite.

In an attempt to simulate the fast cooling of the plasma-arc spraying process, a sample of the fine cobaltate powder was annealed in air at 1300°C for 8 hours, heated to 1430°C and quenched in water. After calcining at 600°C to remove any hydrated phases that might have formed, the powder was analyzed by XRD. Figure 14 shows that the material was essentially pure perovskite after quenching, although the peaks were not as distinct, reminiscent of the less sharp peaks found for the as-sprayed material in Figure 11. Heating in a closed crucible, in air, as opposed to the reducing environment found in the argon–hydrogen gas stream of the plasma, may cause the difference. This was looked at in more depth by performing a simultaneous TG/DTA on the fine cobaltate powder. The sample was heated in an alumina crucible (instead of platinum) at 10°C/min up to 1430°C, and cooled at the same rate to ~500°C.

As shown in Figure 15, the TG curve on heating exhibited a weight loss at 375°C, while the DTA curve for the same region showed evidence of a broad endotherm. These effects may be ascribed to the loss of surface and hydration water. The TG and DTA heating curves were very similar at high temperatures to those of Figures 3 and 9, with both a sharp weight drop and corresponding endotherm at 830°C. There is also an accelerated loss in weight at temperatures above 1200°C, as well as a steep endothermic trend above 1350°C. It is interesting to note that on cooling the sample did not gain weight quickly at temperatures near the melting point. The total weight loss was also less than that for the samples tested in the simulated exhausts. This indicates that in low partial pressures of oxygen, as is the case in the simulated exhaust gas environment, the loss and gain of oxygen is reversible, but that some irreversible process, perhaps the volatilization of cobalt or another of the cations, is at work. At 200°C the appearance of a sudden spike in the TG heating curve is most probably a machine artifact, as is the discontinuity in the DTA cooling curve between 700°C and 600°C.

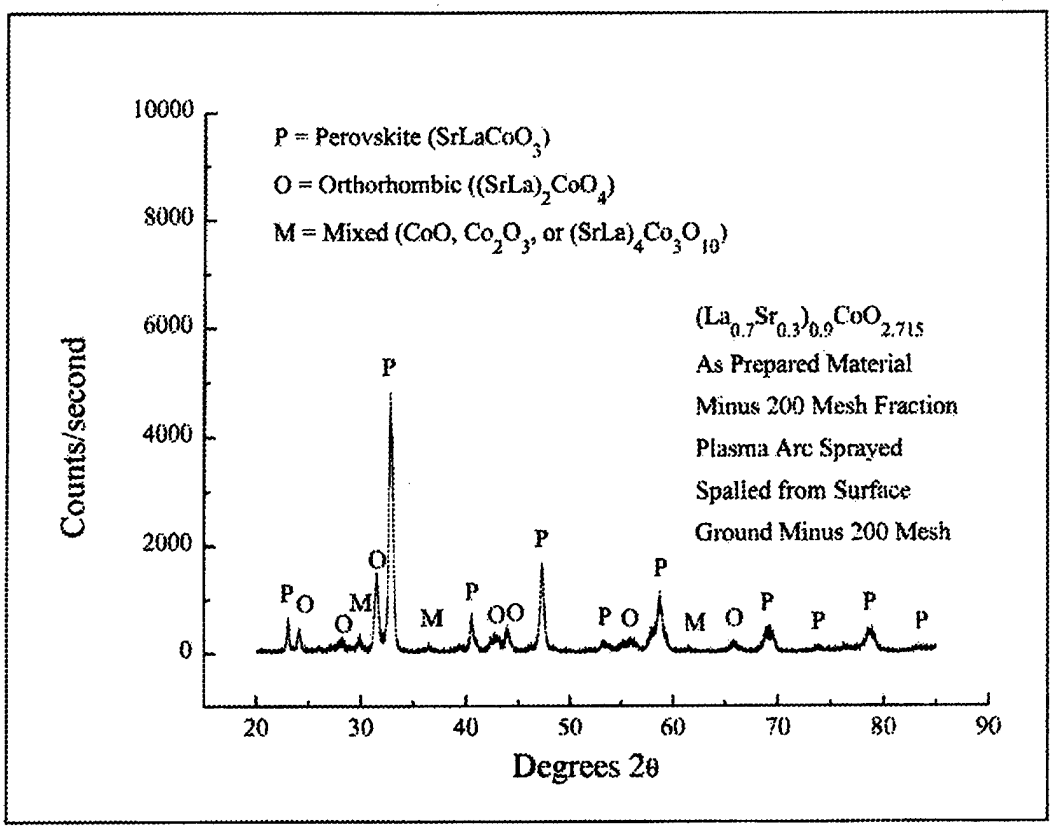

Figure 11: XRD pattern of $(SrO_3La_{0.7})09CoO_{2.715}$ fine calcined powder, plasma-arc sprayed on a zirconia substrate and removed.

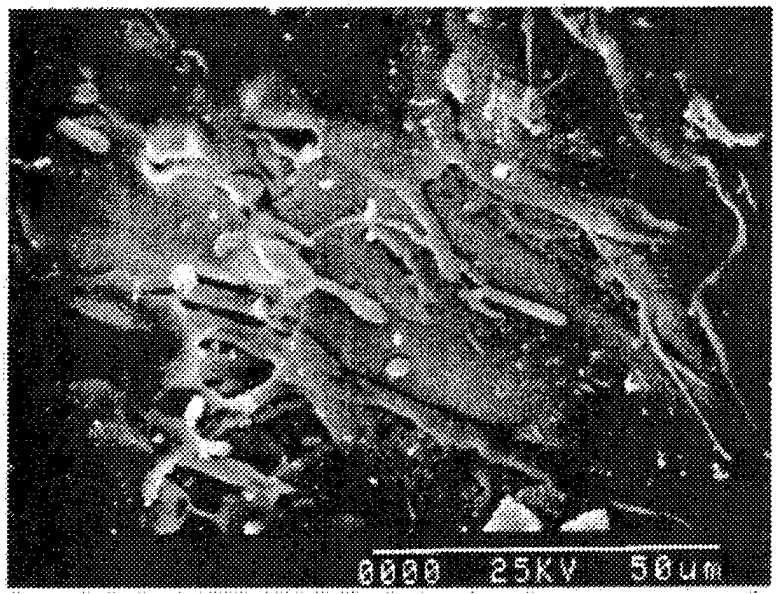

Figure 12: SEM micrograph of fine cobalte powder plasma-arc sprayed on a YSZ tube. Magnification at 950X.

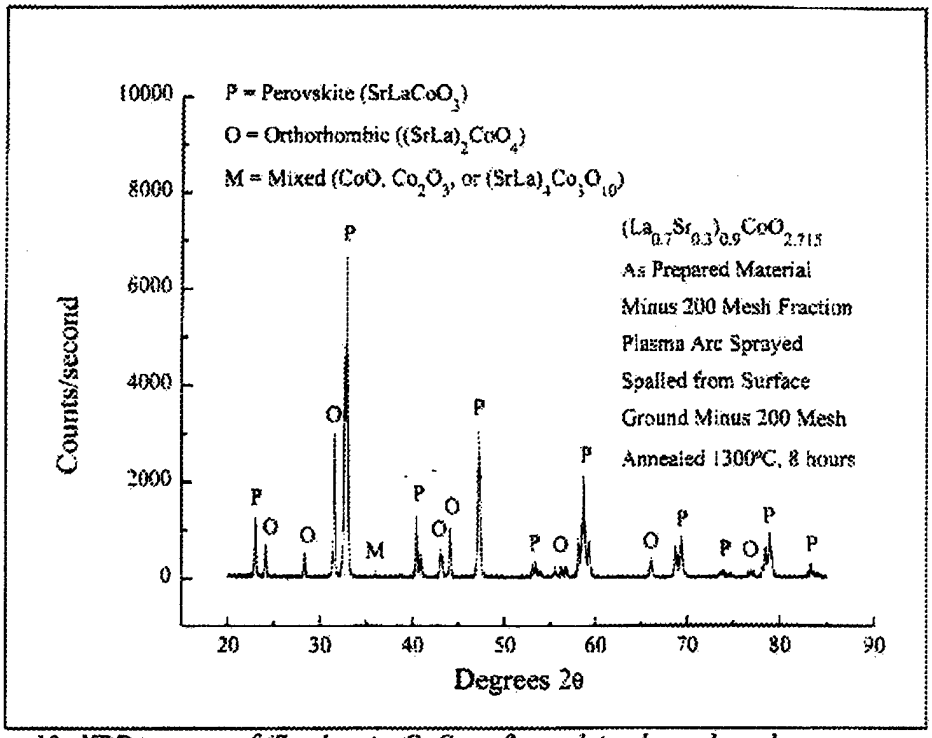

Figure 13: XRD pattern of $(Sr_{0.3}La_{0.7})_{0.9}CoO_{2.715}$ fine calcined powder, plasma-arc sprayed on a zirconia substrate, removed, and annealed 8 hours at 1300°C.

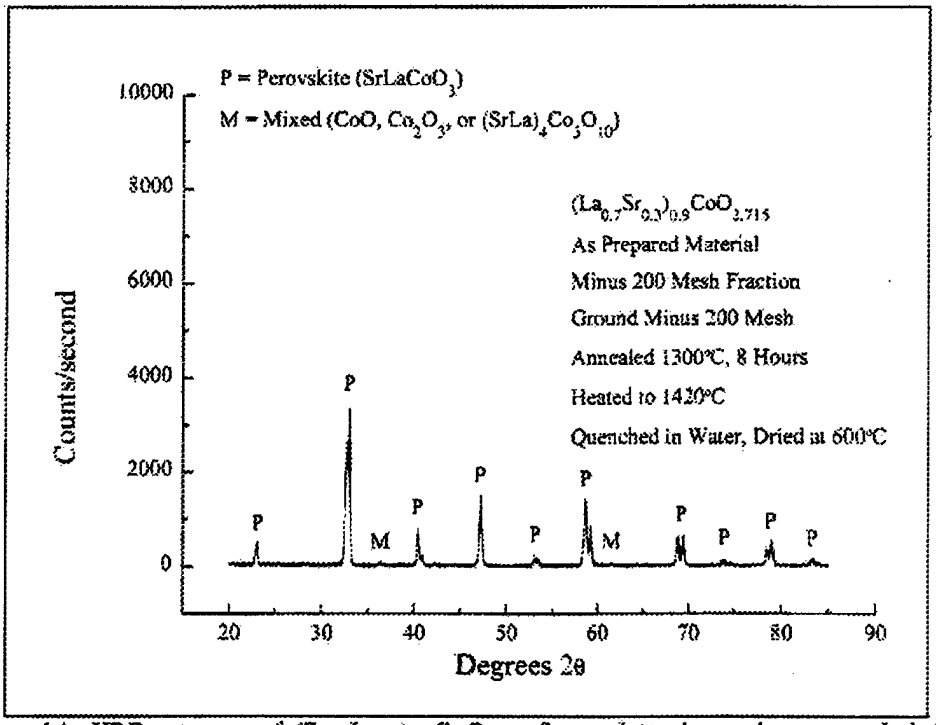

Figure 14: XRD pattern of $(Sr_{0.3}La_{0.7})_{0.9}CoO_{2.715}$ fine calcined powder, annealed for 8 hours at 1300°C, heated to 1420°C and quenched.

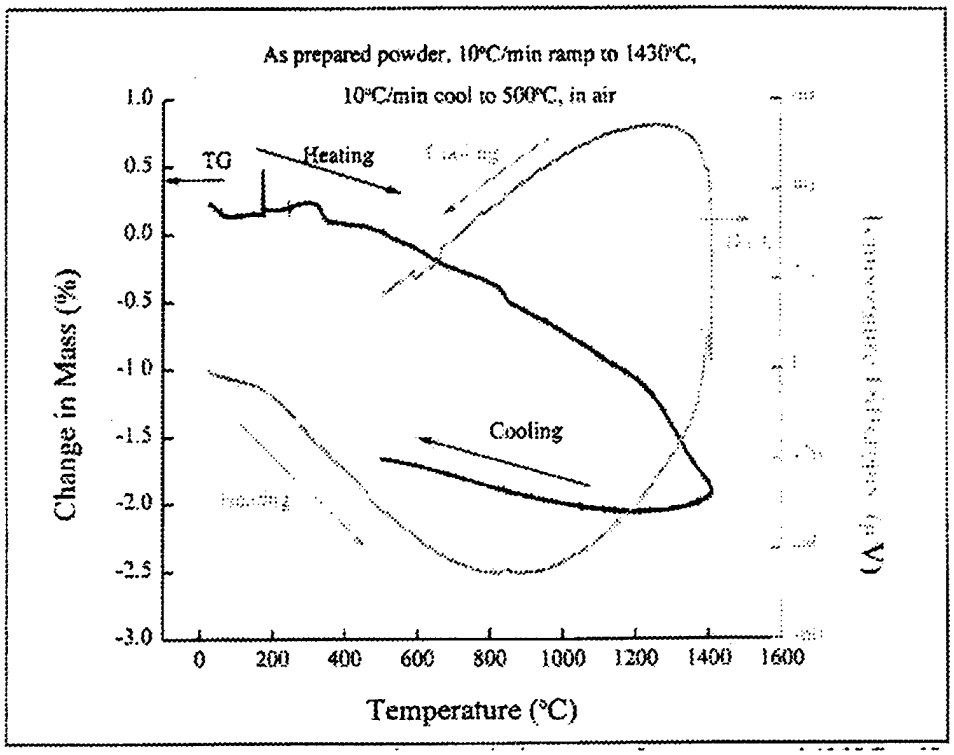

Figure 15: Simultaneous TG/DSC of fine cobaltate powder in air to 1430°C. Heating and cooling at 10°C/min. No dwell.

3. Reactivity of Gases with Plasma-arc Sprayed Coatings

For a material to truly be a catalyst, it must participate in a reaction but be essentially unchanged by it. This essential property has led to the concept of a catalytic cycle, in which reactants are transformed into products by the catalysts There is an uninterrupted, repeating cycle of elementary reaction steps, and the reactants become products through a sequence of reaction intermediates. At the end of the cycle the catalyst is regenerated in its original form. It is the turnover rate of the catalytic cycle that is the fundamental quantitative kinetic quantity sought in studies of catalytic activity. Frequently this information is not directly obtained from experiments, as the quantity known as the site time yield (molecules of product produced per site per unit time) is usually reported. Oftentimes a determination of the number of active sites is the most difficult measurement of all, the number of molecules of product produced (or reactant consumed) per unit time being a comparatively simple quantity to get. It is also not always easy to unequivocally determine the elementary reaction steps involved in the catalytic cycle.

For the reduction of NO by anion deficient strontium doped lanthanum cobaltates in the presence of CO, the catalytic cycle is not yet known. However, a working model of the cycle can be constructed from evidence in the literature. Since catalyst, CO and NO are apparently involved in the reaction it is instructive to look at each of these in turn.

Teraoka, *et al.*[16] investigated the loss of oxygen with temperature from Sr substituted $LaMO_3$ (M = Fe, Co, Mn) perovskites. Using temperature programmed desorption (TPD), two

distinct oxygen desorption peaks were found. The lower–temperature peak was ascribed to desorption of oxygen in oxygen vacancies, while the higher-temperature peak was considered to be the loss of lattice oxygen. Using x-ray photoelectron spectroscopy (XPS) on a series of Sr, substituted lanthanum cobaltates, Yamazoe, *et al.*[15] found two distinct types of oxygen, which they ascribed to adsorbed and lattice oxygen. Pena, *et al.*[15] assigned similarly obtained XPS peaks to lattice oxygen (as O^{2-}) and adsorbed oxygen (as 0^{-}). Nakamura, *et al.*,[25] measured the amount of Co^{3+} and Co^{4+} in as-prepared $Sr_{0.}2La_{0.8}CoO_{3-\delta}$ by wet chemical methods and found the oxygen deficiency was essentially zero, with charge neutrality having been accommodated by 20% of the Co^{3+} having changed to Co^{4+}.

Viswanathan and George[26] found that the oxidation of CO on a series of lanthanide cobaltates was a Langmuir–Hinshelwood type reaction between two adsorbed species, specifically, CO adsorbed on cations adjacent to oxygen vacancies in which oxygen had adsorbed. Nakamura, *et al.*,[25] found that increasing the amount of Sr in Sr–substituted lanthanum cobaltates increased both the amount of oxygen desorbed by TPD and the amount of oxygen desorbed by reaction with CO. In both experiments the oxygen was reversibly desorbed, oxygen having been readily adsorbed back into the lattice with subsequent heat treatment in oxygen.

Voorhoeve, *et al.*[4] determined that when the A site binding energy with surface oxygen was strong, the reactivity of $LaMnO_3$ toward NO reduction was reduced. Thus, the ease of release of oxygen from the lattice was seen as an important factor in NO conversion to N_2. The authors also felt that oxygen vacancies either strongly contributed to or participated in NO reduction. In addition they found through infrared spectroscopy (JR) that NO was molecularly adsorbed as mononitrosyls, dinitrosyls and nitrates. They concluded that NO was dissociatively adsorbed on oxygen vacancies. Tascon, *et al.*[9] found that preadsorption of NO on $LaMO_3$ (M = Cr. Mn, Fe, Co, Ni) perovskites was more inhibiting of later CO adsorption than the reverse process of CO preadsorption followed by NO adsorption. Through IR spectroscopy they found isocyanate (NCO^{-}) and N_2O adsorbate species. Peña, *et al.*[10] found NO to be more tightly adsorbed than CO on La:MnO_3, and that NO adsorbed as dinitrosyis and nitrates.

Based on these observations the following sequence of reactions for the reduction of NO on a perovskite catalyst in the presence of CO is being proposed:

$$NO(g) + * \quad NO*$$

$$NO* + NO(g)* \quad ON*NO$$

$$2CO(g) + * \quad 2CO*$$

$$ON*NO + CO* \quad CO_2* + ON*N$$

$$ON*N + CO* \quad CO_2* + N_2$$

$$2CO_2* \quad CO_2(g) + *$$

$$N_2* \quad N_2(g) + *$$

where the (g)'s are gas phase species, and the *'s are surface sites. At this time it is not certain whether these sites are associated with cobalt, oxygen defects or vacancies, or some combination of both, or for that matter, whether NO and CO adsorb on similar sites.

The first three are adsorption reactions, the next two are surface reactions, and the last two are desorption reactions. It is generally thought that adsorption of reactants and desorption of products are fairly quick reactions, but that desorption of the ON*NO and CO* adsorbed species and the surface reactions are rate controlling.[27] The surface reaction depends on the time that the reacting species spend on the surface, usually characterized by the mean residence time. In order to begin to investigate the fundamental catalytic reaction cycle for surface catalyzed reduction of NO in the presence of CO, heat effects associated with adsorption and reaction of NO and CO in the presence of a perovskite coating were observed using a DTA technique. Using an alumina DTA crucible plasma-arc sprayed with the fine cobaltate powder as the sample and an alumina crucible as the reference, the couple was heated in flowing helium to a set temperature. After a short dwell period during which the temperature of the system was allowed to stabilize, the helium flow was shut off and replaced by flowing 10% NO in N_2. Some minutes later, after an adsorption isotherm was observed and the reference temperature had stabilized, 10.5% CO in CO_2 was mixed with the 10% NO in N_2 gas stream. An exothermic effect at this point was considered to be due to a surface catalyzed reduction of NO in the presence of CO. After both the heat effect and reference temperature became stable again, the reactive gases were shut off and helium again introduced to the sample chamber. The temperature was ramped to a new set point and the process repeated. This technique was employed at set points ranging from 400°C to 1200°C, in 100°C steps. Figure 16 shows a typical heating ramp and DTA curve for this series of tests. The adsorption and reaction exotherms are evident in the plateau regions of the DTA curve. There are also subtle changes in the reference temperature corresponding to those exotherms. During the temperature ramps there is an apparent, and large, exothermic effect. This may be tentatively attributed to a difference in emissivity between the metallic oxide perovskite coating on the outside surface of the sample crucible, and the uncoated alumina reference crucible. Metals generally have higher emissivities than alumina, and would therefore heat up at a much higher rate, all other things being equal.

The adsorption/reaction plateau region thermograms for five of the setpoint tests are shown in Figure 17. The 10% NO in N_2 gas was introduced in the first couple of minutes (there was some lag as the gas went from the valve to the chamber), and the 10.5% CO in CO_2 some 20 minutes later. There was a definite early exotherm at both 400°C and 600°C, which has been associated with the adsorption of NO. It is difficult to pick out a similar effect at higher temperatures, but the decrease in signal from 400°C to 600°C indicates a trend toward the lack of effect observed at higher temperatures. When CO was introduced to the gas stream, another, more significant, exothermic effect was observed, and it apparently decreases with increasing temperature. This effect was ascribed to the surface reaction of NO with CO to produce N_2 and CO_2.

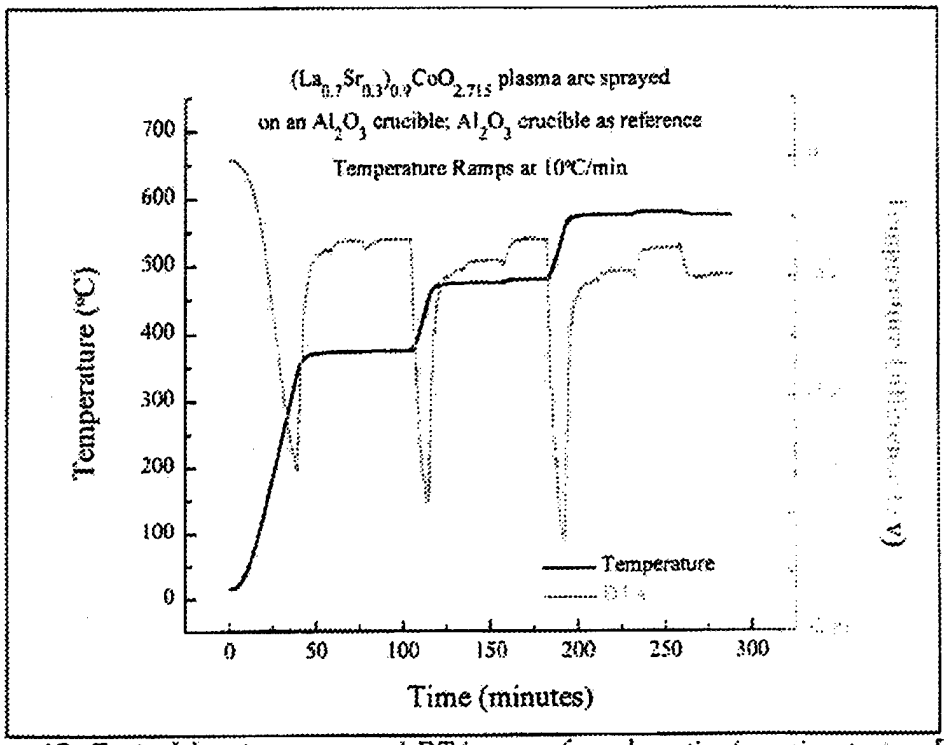

Figure 17: Typical heating ramp and DTA curve for adsorption/reaction tests. Large apparent exotherms during heating are due to high emissivity of metallic oxide coating.

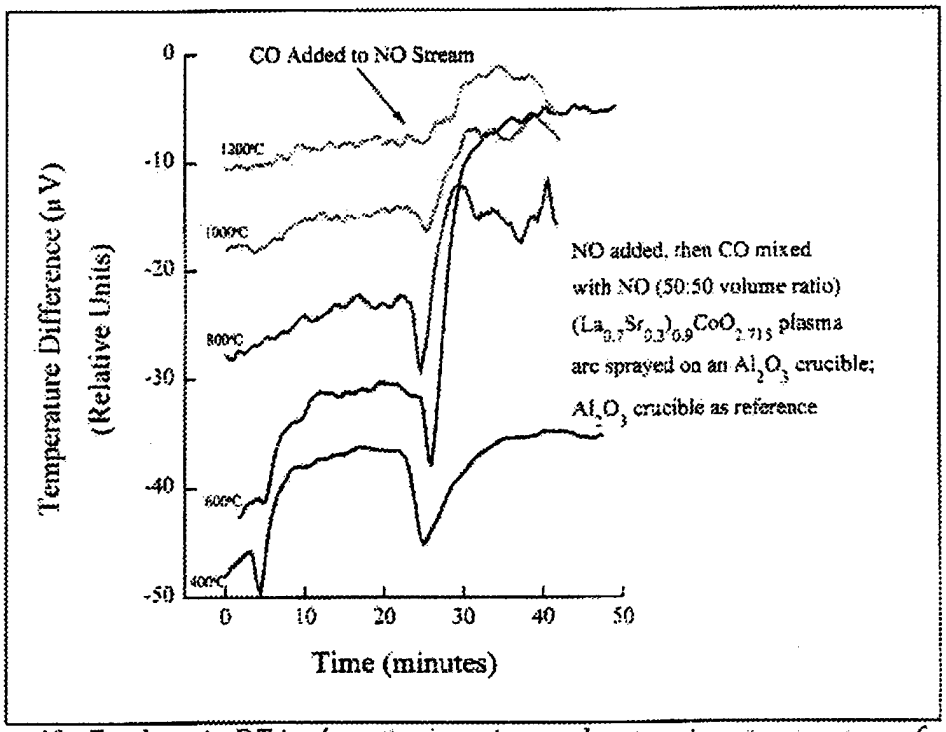

Figure 18: Exothermic DTA adsorption/reaction peaks at various temperatures for fine cobaltate powder plasma-arc sprayed onto an alumina DTA sample crucible.

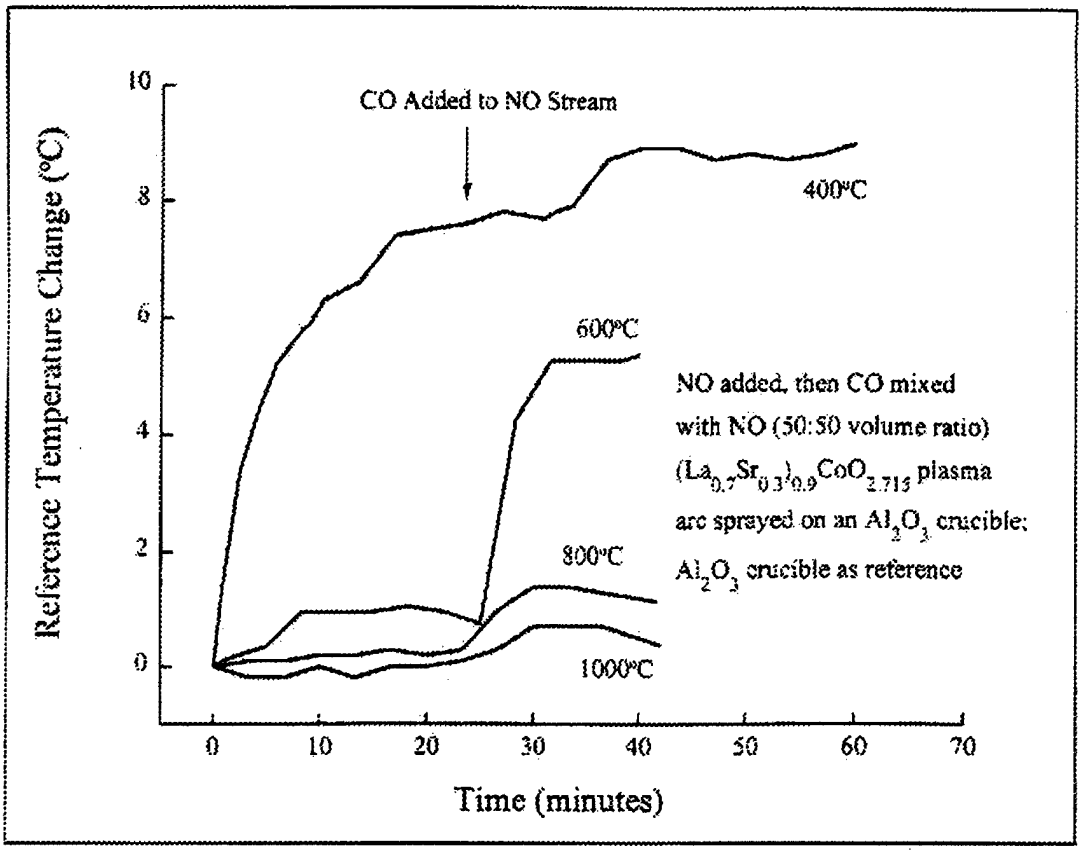

Figure 19: Increase in DTA chamber reference temperature upon introduction of NO and NO and CO gas mixtures.

The apparent endothermic effects observed after the exotherms can be explained with reference to Figure 19, which shows the increase in reference temperature during the same time periods as are plotted in Figure 18. From Figure 17 it can be seen that the sample temperature was always higher than that of the reference, even when the system was in a dwell period. While these reactions were occurring the reference temperature increased and became closer to that of the sample crucible, giving the false impression of an endotherm. Again referencing Figure 19, it is important to note that the temperature rise at the 400°C setpoint was continuous. This is most likely due to the reaction of NO with any available O_2 to form NO_2, which is actually the dominant oxide of nitrogen at low temperatures. Whether this reaction was surface catalyzed is not known at this time. The significant rise in reference temperature during the 600°C setpoint dwell could be due to either a surface catalyzed reaction or a bulk gas phase reaction. This technique seems to hold much promise for delineating the catalytic cycle involved.

4. Laboratory Scale Reactors

Two bench scale reactors for the evaluation of high temperature catalytic properties of the prepared cobaltate material were designed and constructed. The reactors were designed to test the catalyst in different gas mixtures, simulating combustion exhaust gas streams.

The fluidized bed apparatus consists of a kanthal wound furnace, capable of temperatures to 1200°C, with concomitant furnace tube, gas phase connections and temperature controller. Figure 20 shows a schematic representation of the experimental cell (reactor). The

present configuration is set up to simultaneously measure the NO_x content of gases passed through the catalyst powder and the oxygen partial pressure of the catalyst surface in contact with the gas stream. The oxygen potential measurement is accomplished by using a closed end yttria stabilized zirconia (YSZ) tube as the sample holder, electroding the exterior of the closed end with platinum, and making electrical connection to the electrically conductive catalyst powder as the other electrode of an electrochemical cell. The catalyst powder is placed in the reactor tube and the tube is sealed with a metal end cap through which gases are fed and electrical leads to thermocouples and the catalyst powder itself are supplied. The electrically conductive catalyst thus functions as the anode in an electrochemical cell with the reactor tube as the solid electrolyte and the ambient air at the platinized surface as the reference cathode. A chemiluminescence $NO\text{-}NO_2\text{-}NO_x$ analyzer (Thermo Environmental Instruments, Inc., Model 42H) was used to measure the nitrogen oxide content of the gases after passing through the catalyst. The gas stream composition entering the reactor is controlled via external flow meters. The emf between Pt process electrode wire and the Pt air electrode wire, corresponding to the oxygen potential difference between the catalyst and the ambient air, is monitored by an external electrometer. In addition to performing

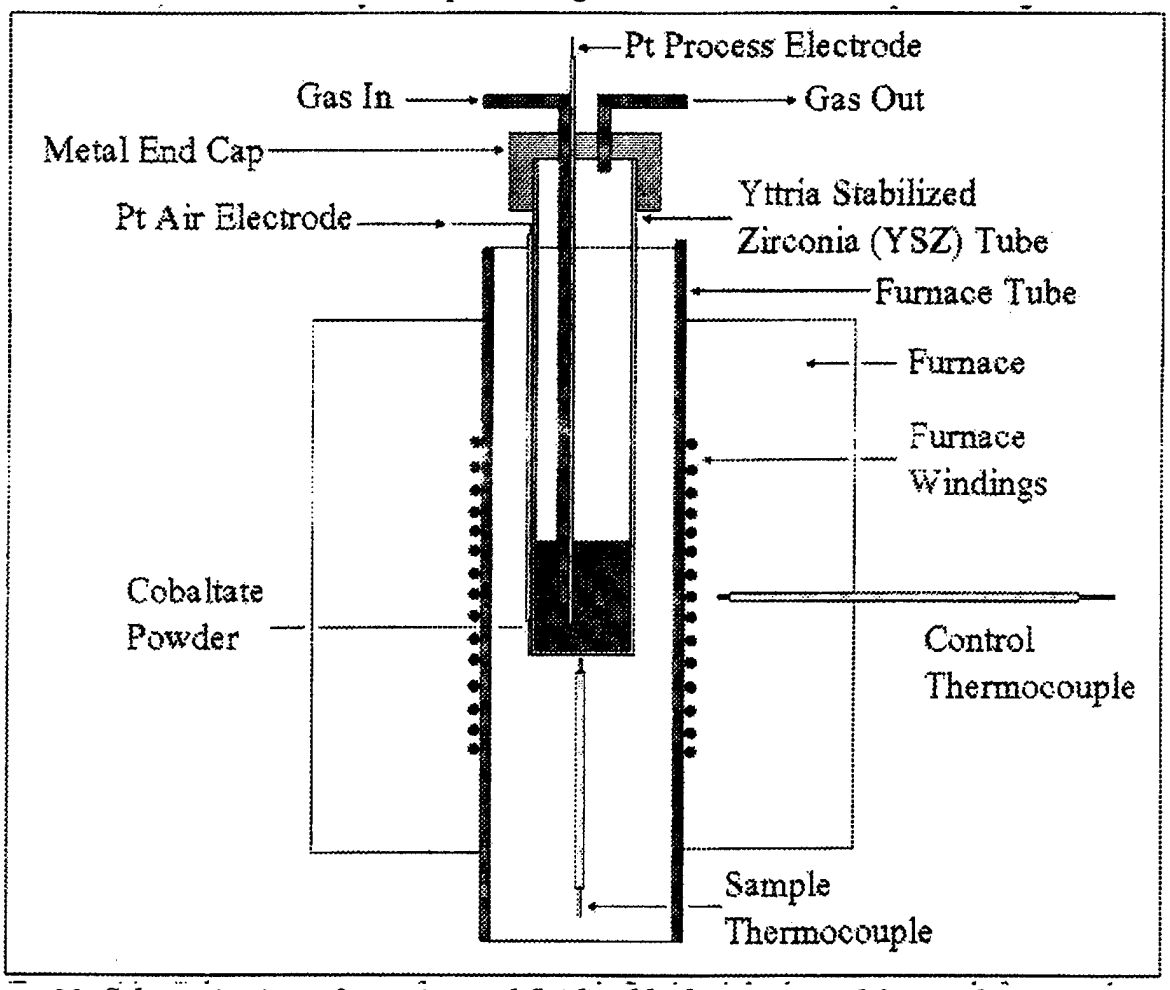

Figure 20: Schematic view of experimental fluidized bed reactor used for catalytic measurements.

electrochemical measurements to monitor the state of the catalyst, the cell is designed to permit control of the chemical reactions occurring on the catalyst by imposing a fixed oxygen potential on the catalyst.

Figure 21 is a schematic of the design for a higher space velocity reactor. A YSZ tube with a plasma-arc sprayed coating of the cobaltate catalyst will act as the reaction substrate and the electrochemical cell. The substrate will be inside a close fitting outer tube of Al_2O_3, which will allow somewhat higher velocity gas contact with the catalyst. Electrochemically, the cell will be reversed from the configuration of Figure 20, with the exhaust gas passing over the external surface and the air reference electrode being on the internal platinized surface of the stabilized zirconia substrate tube.

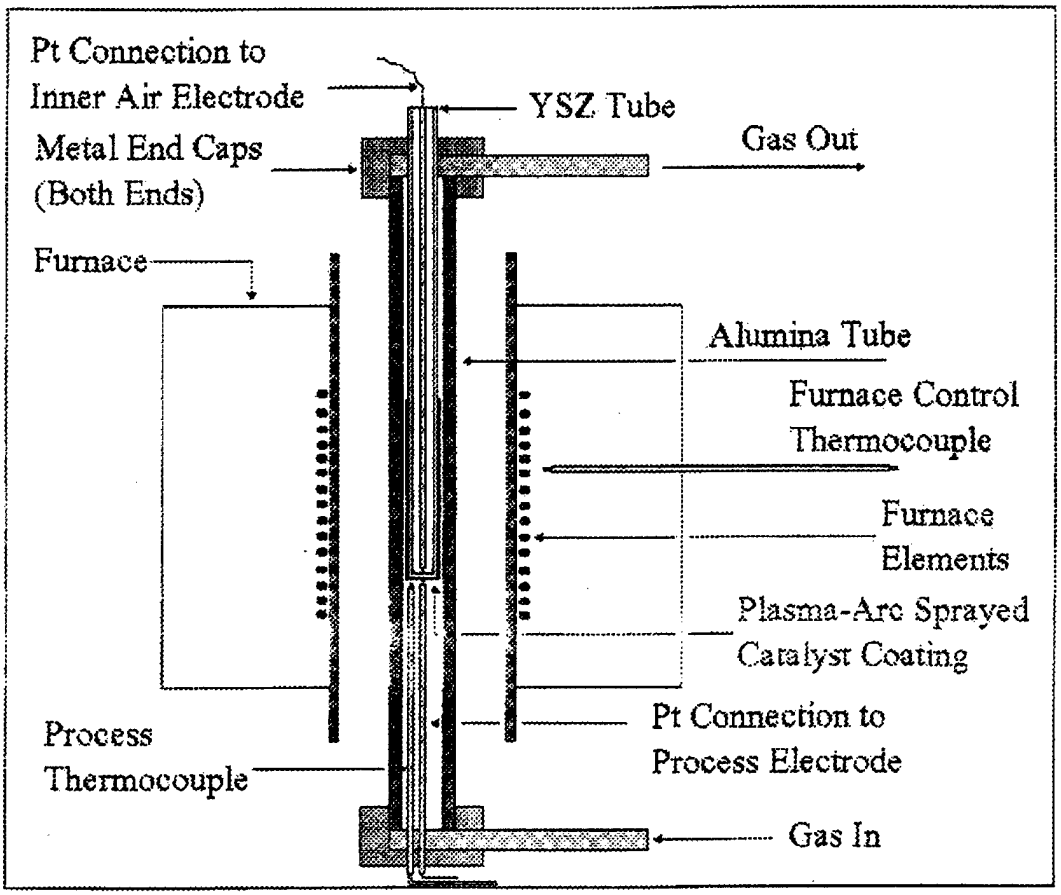

Figure 21: Schematic of modified reactor to accommodate higher gas flow rates over plasma-arc sprayed catalyst coatings.

As currently configured, the laboratory scale fluidized bed reactor assembly has a space velocity of ~1 sec^{-1}, and a dwell time of ~1 sec. The annular tube reactor has a limiting space velocity of 70 sec^{-1}, and a dwell time of 15 msec. It is difficult to determine the average contact time of a molecule with a catalyst surface if the conditions of a continuous, well-stirred reactor are not realized. For the laminar flow of a gas across a surface, only a percentage of the molecules will come into contact with the catalyst. Turbulent flow at high temperatures increases the chance of contact with the surface, but in either case attempting to quantify the percentage of the gas stream contacting the surface would yield only an approximate result. A

jet engine, with rapidly spinning turbine blades, may be a good approximation of a continuous, well-stirred reactor, with every molecule having an encounter with a surface site, but the duplication of those conditions in a laboratory are difficult.

5. Equilibrium Calculations

It has been shown that significant concentrations of NO can be converted to N_2 at relatively low temperatures when reducing conditions are maintained with CO/CO_2 buffers. However, it has been emphasized that the behavior of these catalysts under conditions of high temperatures (900-1600°C) and small amounts of NO (typically 50 ppm and below) is the preferred area of investigation. To initiate this area of investigation, computer calculations to determine equilibrium compositions at various temperatures were performed for several gas compositions using a commercial software program (Outokumpu HSC Chemistry for Windows, ARS Software Corporation, Landover MD). The purpose of this phase of the investigation was to determine what levels of NO reduction are thermodynamically possible. Once this is known, then the degree to which the catalyst can enhance the kinetics of the reduction can be determined.

As a starting point, a gas with a composition of 50 ppm NO in N_2 was used as the input. Figure 22 shows the results of the equilibrium calculations for temperatures from 25°C to 1300°C. While the amount of NO present increases with temperature, it is important to note that the calculated equilibrium concentration of NO at 1300°C is 18 ppm, a significant drop with respect to the starting concentration of 50 ppm.

Next, the effect of water on the equilibrium concentration of NO was calculated. Figure 23 shows the equilibrium concentrations of NO and O_2 at 1100°C, 1200°C and 1300°C for a starting gas composition of 50 ppm NO in N_2 with from 1 ppm to 2.4% H_2O. Increasing the temperature increases the equilibrium concentration of NO, but again it is less than the starting concentration of 50 ppm.

Figure 24 shows the calculated effect. of small concentrations of CO on the equilibrium NO and O_2 concentrations at 1100°C, 1200°C and 1300°C, for a starting composition of 50 ppm NO with additions of CO from 5 to 100 ppm. At CO concentrations below the starting NO concentration of 50 ppm, the O_2 concentration does not change significantly, resulting in little reduction of NO beyond the NO/N_2 equilibrium levels. At greater than 50 ppm CO there is a significant drop in O_2 concentration, with the concomitant decrease in NO. The effect is less drastic with increasing temperature.

The final calculation performed in this series was for a starting mixture of 50 ppm NO in N_2 with 2.4% H_2O, with the concentration of CO varying between 5 and 100 ppm. In Figure 25 the effect of CO is mitigated under this wet condition, with less significant decreases in the equilibrium concentration of O_2

All of these calculations indicate that when small amounts of NO are present in the exhaust of a high temperature (1600°C) combustion process, the equilibrium quantity of NO is quite low at the temperatures below which this catalyst is stable (<1350°C). Small amounts of CO, whether introduced after the fact or as residuals of an incomplete combustion process, have the potential for promoting significant NO reduction.

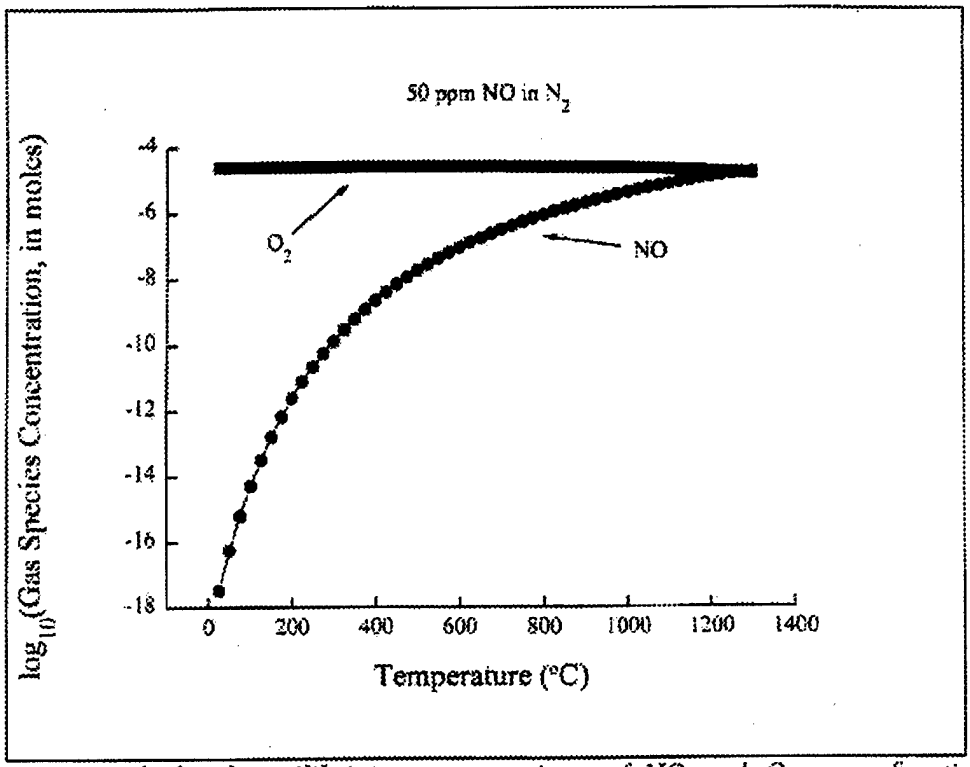

Figure 22: Calculated equilibrium concentrations of NO and O_2 as a function of temperature for a starting gas composition of 50 ppm NO in N_2.

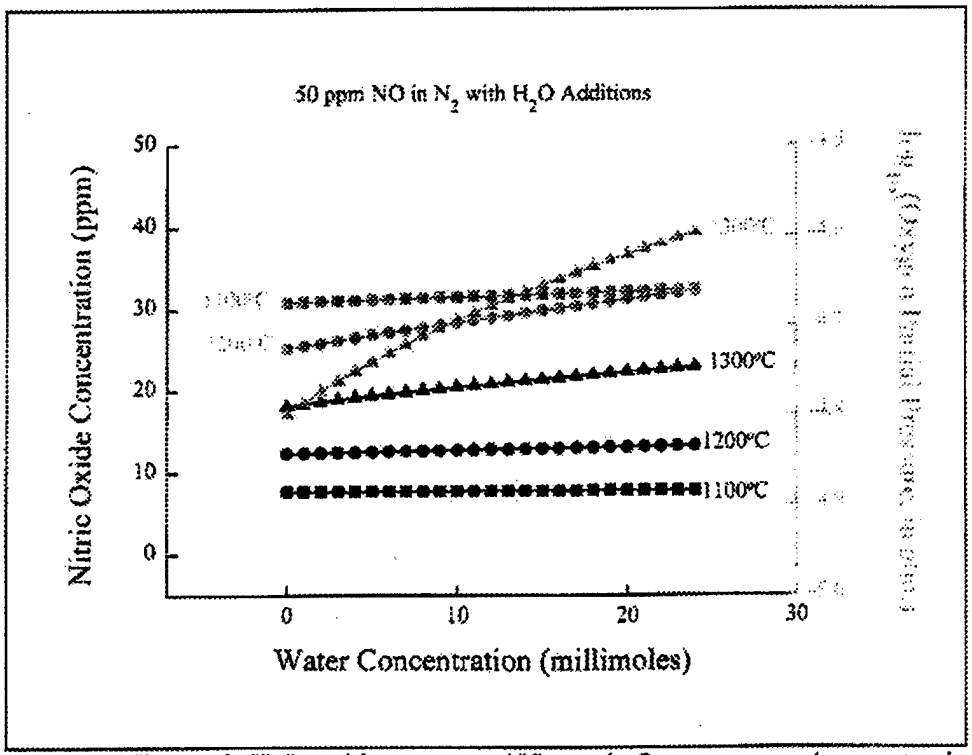

Figure 23: Effect of H_2O additions on NO and O_2 concentrations at elevated temperatures for 50 ppm NO in N_2.

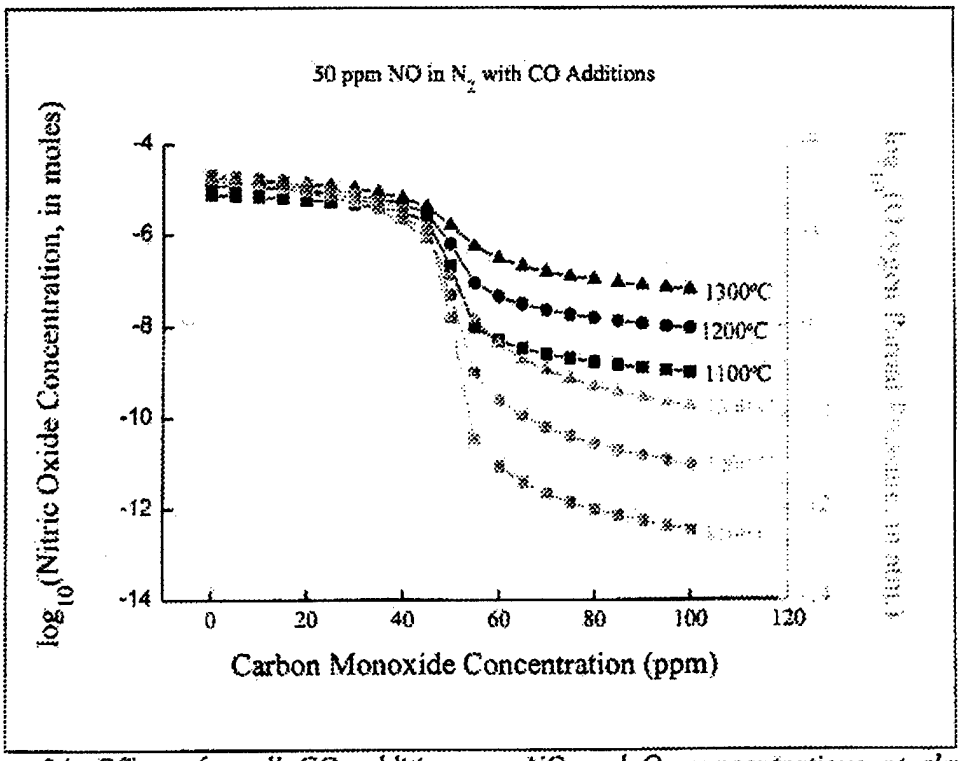

Figure 24: Effect of small CO additions on NO and O_2 concentrations at elevated temperatures for 50 ppm NO in N_2.

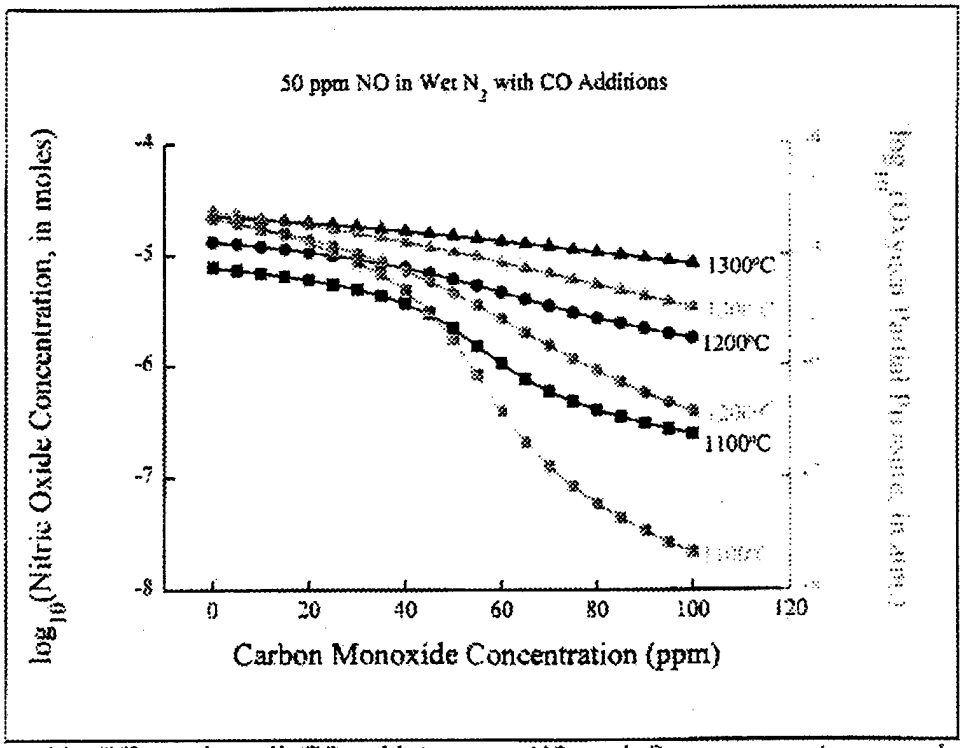

Figure 25: Effect of small CO additions on NO and O_2 concentrations at elevated temperatures under "wet" conditions.

6. Evaluation of Catalyst Efficiency

a) Preliminary fluidized bed reactor tests

The literature attests to the fact that strontium doped lanthanum cobaltate is an active catalyst for NO_X reduction, as documented earlier in this report. The conditions under which this would be true were investigated by measurements carried out on a tank gas composition consisting of nominally 1013 ppm of NO with the balance nitrogen. This gas was also mixed with up to 60% air prior to passing through the reaction chamber. NO, NO_2 and NO_X values were measured with the Thermoluminescence NO_x Analyzer, which gives concentrations in ppm. Since the pressure inside the reaction chamber is approximately 1 atmosphere, these data may be converted to partial pressures in atmospheres A concentration of 1000 ppm in the gas cylinder thus converts approximately to 10^{-3} atmospheres in the reaction chamber. The oxygen partial pressure was measured electrochemically. These P_{O_2} data are more readily expressed in atmospheres, and since the range of variation is great, it is convenient to plot them on the right hand axis on a logarithmic scale as shown in the Figures.

Figure 26 shows data recorded after passing the gas through the fluidized bed reaction chamber without any catalyst powder. At low temperatures the NO was oxidized to NO_2, a not surprising effect considering that NO2 is the major nitrogen oxide species at low temperatures. The calculated value of log P_{O_2} is -0.898 for the incoming gas in Figure 26. As can be seen in Figure 26, this is near the value measured at low temperatures, but much greater than that measured at temperatures above 400°C.

Figure 27 shows the effect, with respect to temperature, of the catalyst powder on the concentrations of NO, NO_2, NO_X and O_2 for the 1013 ppm NO in N_2 feed gas. A significantly greater amount of NO was converted to NO_2 at low temperatures in the presence of the catalyst, but no reduction of NO took place. The calculated value of log P_{O_2} for the incoming gas, -0.898 corresponds very well to the measured value after passing through the catalyst powder at temperatures above 600°C. The baseline oxygen partial pressure in Figure 27 cannot be readily estimated, because the oxygen partial pressure in the NO/N mixture is unknown, and the catalyst would give up some oxygen at very low partial pressures.

When extra O_2 (as air) was added to the 1013 ppm NO in N_2 input gas, the P_{O_2} measured was raised, as can be seen in Figure 28. The relative behavior of NO and NO_2 in the catalyst bed was similar to that found in Figure 27.

Important points to be noted from these three Figures include the fact that the measured NO_X concentration is equal to the sum of the measured NO and NO_2 concentrations, and that while the NO/NO_2 ratio varies as a function of temperature, the total NO_x concentration remains sensibly constant.

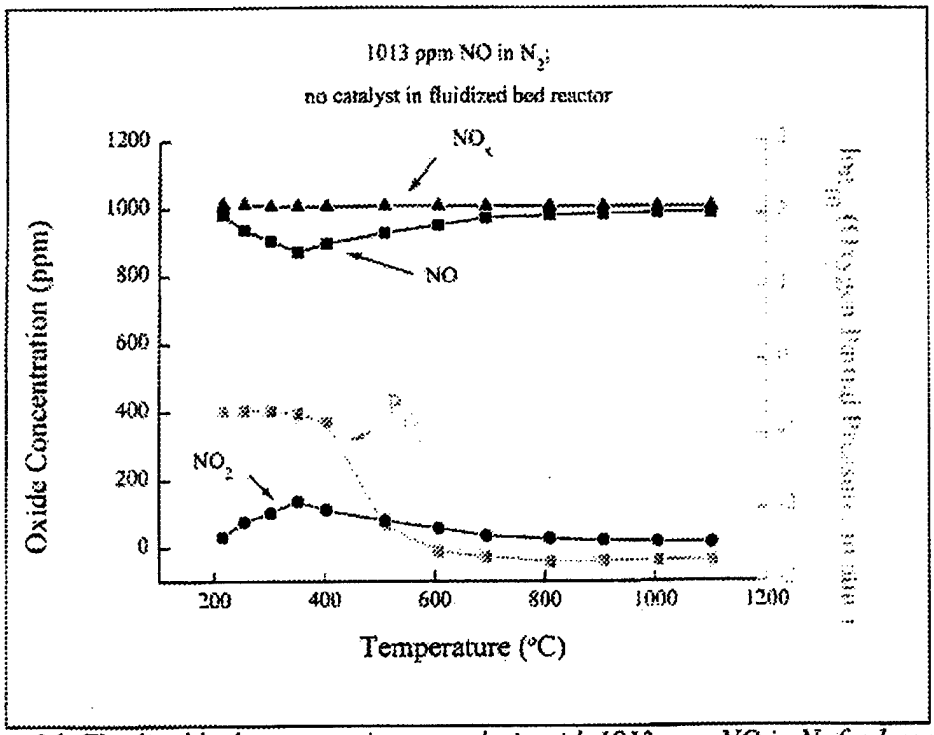

Figure 26: Fluidized bed reactor exit gas analysis with 1013 ppm NO in N_2 feed gas. No cobaltate powder in bottom of reactor tube.

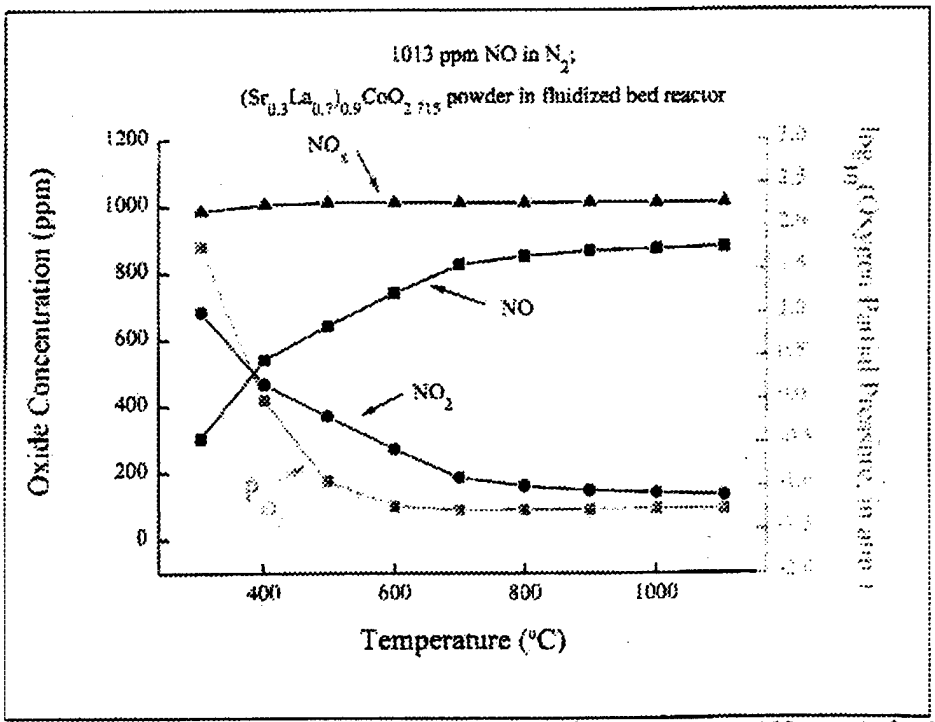

Figure 27: Fluidized bed reactor exit gas analysis with 1013 ppm NO in N_2 feed gas. Fine cobaltate powder in bottom of reactor tube.

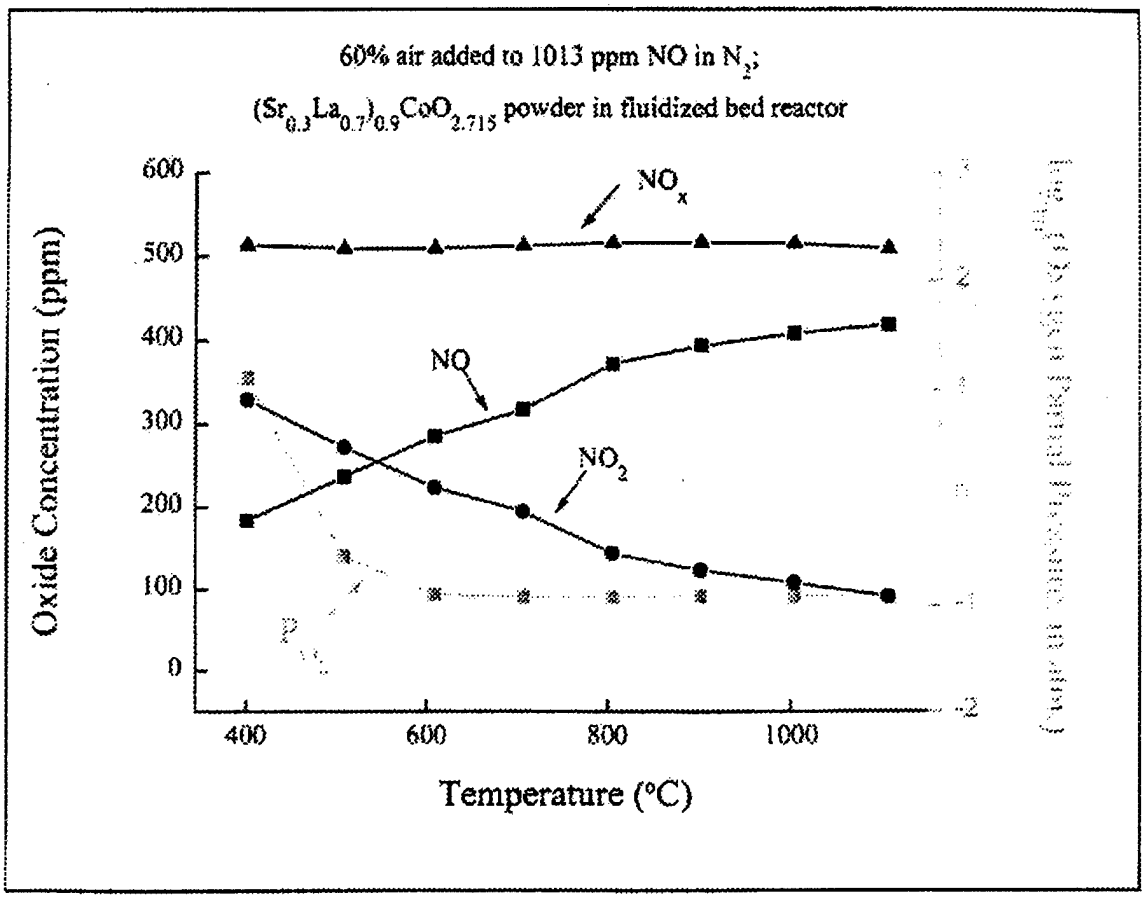

Figure 28: Reactor exit gas analysis with 60% air added to 1000 Pam NO in N2 feel gas. Fine cobaltate powder in bottom of reactor tube.

It is clear from the results shown in the three previous Figures that NO_x is not reduced by the strontium lanthanum cobaltate catalyst when the only constituents of the gas phase are nitrogen, oxygen and oxides of nitrogen. NO is probably not dissociatively adsorbed on the catalyst under these conditions, and this dissociation would be necessary for the direct reduction of NO on the catalyst.

When CO was added to the NO/N_2 mixture, the results were quite different. Approximately 20% of a 10% CO in CO_2 gas was added to the 1000 ppm NO in N_2 gas, and this mixture was run through the catalyst powder in the manner of the previous experiments, with very notable results, as shown in Figure 29. At about 250°C the NO was completely reduced. The oxygen partial pressure on the catalyst, measured electrochemically, went through a minimum near the temperature at which the NO disappeared, then increased gradually as temperature was increased. The reaction that was being catalyzed is apparently:

$$2NO + 2CO = N_2 + 2CO_2$$

The second observation of significance is that the reaction goes to completion at a very low temperature (250°C). This would obviate the need to place the catalyst in the very high temperature region of the exhaust stream. The structural and chemical stability constraints on the

catalyst system could be greatly alleviated by low temperature operation. It would also promote more complete reaction insofar as the NO_X is stable at high temperatures. The equilibrium concentration of NO_X would increase with increasing temperature, and the catalyst can only promote equilibrium by providing a reaction path with lower activation barriers.

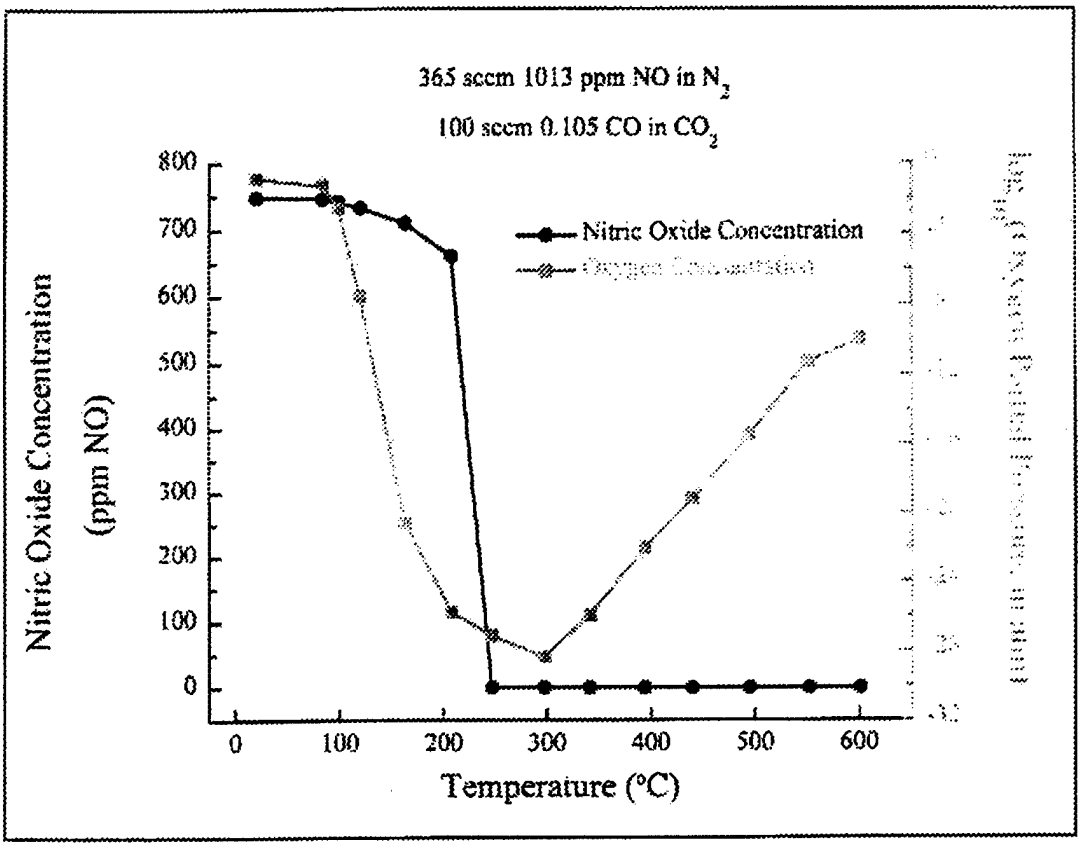

Figure 29: Fluidized bed reactor exit gas analysis for 20% of 10.5% CO in CO_2 with 1013 ppm NO in N_2 input gas.

b) Annular reactor tests

Higher space velocity tests were carried out in the annular reactor, shown schematically in Figure 20, both with and without a catalyst coating on the outside of the zirconia tube. Because plasma sprayed coatings could not be retained on the surface of the zirconia tubes due to the large mismatch in thermal expansion coefficients, it was decided to coat the tubes with an ink made from an organic carrier and the perovskite catalyst powder. This ink was formulated by grinding together in a mortar approximately 50% by volume of the perovskite catalyst powder with 50% by volume of an organic carrier consisting of 25% tert-butanol (2-methyl propanol), 25% methyl ethyl ketone (MEK, 2-butanone) and 50% two-part epoxy resin. This ink was brushed onto a 75 mm length of the cylindrical part of the closed end of the zirconia tube. Platinum ink electrodes were painted onto the outside and inside of the closed end cap of the tube. Prior to testing the coated tube was fired for 8 hours at 900°C in air.

The experimental matrix consisted of four variables: T, reactor temperature (400°C to 1300°C in 100°C increments); , stoichiometric ratio, (2 (fuel-lean condition), 1 (stoichiometric) and 0.5 (fuel-rich condition)); nominal NO input concentrations (2, 20, 200. 2000 ppm) and H/C, hydrogen to carbon ratio (1, 2, 3, and 4). A stoichiometric ratio of unity meant that there was just sufficient oxygen to fully oxidize the carbon and hydrogen components to carbon dioxide and water. Twice this amount of oxygen characterized the fuel-lean condition, while the fuel-rich condition meant that only half the stoichiometric amount of oxygen was present. The hydrogen-carbon ratio was varied to simulate different starting fuels. Thus there were 48 gas compositions (3 's x 4 [NO]'s x 4 H/C's = 48) tested at 10 reactor temperatures, for a total of 480 experimental cells.

Batch calculations began by assigning the amount of carbon in all gas mixtures the value of 1. The amount of hydrogen was then determined from the hydrogen-carbon ratio, the amount of oxygen calculated from the stoichiometric ratio, and the nitrogen required to simulate air calculated by multiplying the oxygen content by 78/21, the ratio of nitrogen to oxygen in the atmosphere. The NO input was then added as an extra component. Once all the total quantities of N. C, O. and H were calculated, the gas batches were partitioned into contributions from CO, 10.5% CO in CO_2, 1013 ppm NO in N_2, 10% NO in N_2, N_2, O_2 and H_2 tank gases. All compositions were diluted by a factor of 20 with helium (5% active gases, 95% He diluent). Dilution was required to assure that no explosive mixtures were used and that water vapor did not condense out of the exit gas stream. Condensate would interfere with the chemiluminescence analyzer, and would also contain an indeterminate amount of dissolved nitrogen oxides as nitrous and nitric acids. Implicit in these batch calculations was the assumption that reactions involving the "fuel" and "air" components, namely the carbon monoxide-carbon dioxide and hydrogen-water equilibria, would be so rapid that equilibrium would be achieved readily, while the approach to equilibrium of the nitrogen-oxygen species would be sluggish. Thus simulated exhausts would not have to be batched explicitly, but would be obtained in the reactor. This technique also allowed for more precise and convenient control of the water content.

Table 2 lists the nominal gas input compositions used in these tests, along with the stoichiometric conditions, nominal nitric oxide content and the hydrogen-carbon ratios for each. From rotameter flow tables calibrated for the various tank gases used, settings for six rotameters were selected to achieve the desired compositions at a total flow rate of 2000 sccm. This flow was then divided into approximately three equal parts, one having been sent through the working side of the annular reactor, one through the inside of the zirconia tube and the third either shunted to the exhaust system or sent directly to the NO_X analyzer. Temperatures were measured with a Pt/Pt- 10% Rh thermocouple placed inside the zirconia tube approximately 2 cm from the closed end.

Because of the design of the reactor used in these experiments, three general mechanisms for the conversion of NO to N_2 were anticipated to be operative: a wholly gas phase reaction; a surface catalyzed reaction on the alumina and zirconia components of the reactor; and a surface catalyzed reaction on the perovskite catalyst coating. In order to extract just the effect of the catalyst coating, all experiments were performed twice, once in a blank reactor containing no catalyst and again in a reactor with the catalyst coating. The fraction of NO converted by the blank reactor was determined from the following:

FRACTION CONVERTED BY BLANK =

$$FCB = \frac{\text{INPUT TO BLANK} - \text{OUTPUT FROM BLANK}}{\text{INPUT TO BLANK}} = \frac{IB - OB}{IB}$$

For the reactor with the catalyst coating, the total amount of NO converted is given by:

AMOUNT CONVERTED IN REACTOR WITH CATALYST =

CRC = INPUT WITH CATALYST- OUTPUT WITH CATALYST = IC - OC

For the catalyst only, then:

AMOUNT CONVERTED BY CATALYST =

CBC = CRC – IC(FCB)

Equilibrium compositions were calculated for all 48 starting gas mixtures at temperatures from room temperature through 1300°C. In Figures 29 through 40 the calculated equilibrium concentration of NO and the measured concentration of NO after the starting mixtures had been passed through the reactor with the catalyst coating are plotted against temperature. Each plot contains the data for the four H/C ratios for one and one nominal NO input concentration. The total amount of NO converted and the amount estimated to have been converted by the catalyst are plotted against the reactor temperature for the same combinations of H/C, , and NO input concentration in Figures 41 through 52. A positive number for the amount converted means a reduction in the amount of NO, while a negative number indicates that NO was formed in the reactor.

For fuel-lean conditions (= 2), equilibrium with respect to the NO concentration is rarely achieved. When the input concentration of NO was above the calculated equilibrium amount for a particular gas mixture, the measured amount was above the equilibrium amount. Conversely, when the input concentration was below the equilibrium amount, the measured concentration stayed below the equilibrium amount. In other words, the system was kinetically hindered in its approach to equilibrium. From Figures 29 through 32 it can be seen that, with increasing temperature, the system was, in general, further away from equilibrium. In addition, these Figures also show that an increase in the H/C ratio yielded a closer approach to equilibrium. In Figures 41 through 44 the amount of NO converted in the reactor and the amount calculated to have been converted by the catalyst are plotted against the reactor temperature for the fuel-lean tests. For most compositions and temperatures the amount converted by the catalyst was a small proportion of the already small total amount converted.

For the stoichiometric (= 1) and fuel-rich (= 0.5) conditions, equilibrium with respect to the NO concentration was more readily achieved, as can be seen from Figures 33 through 40. Conversion was 100% efficient at all temperatures and starting compositions, except for the lowest temperatures and the highest input concentrations. However, as is shown in Figures 45

through 52, under those conditions where less conversion took place, a greater percentage of the conversion was attributable to the presence of the catalyst. This means that, under those conditions in which either a gas phase or substrate (ZrO_2 or Al_2O_3) enhanced surface reaction was not particularly efficient, the perovskite catalyst provided a closer approach to equilibrium. The role of the zirconia and alumina reactor materials should be emphasized because of the implication it has for NO_x reduction in high temperature combustion processes, such as are found in jet engines.

Thermal barrier coatings are commonly made of zirconia or alumina, alloyed with other constituents. These present results indicate that properly constituted ceramic thermal barrier coatings employed in high temperature zones would effect significant NO reduction in jet engine exhausts under most conditions. Placing the perovskite catalyst in a lower temperature zone, where it has been shown to be more effective, would provide additional capacity for NO reduction.

Table 2: Nominal gas input compositions, as fractions of total gas input, assuming an ideal gas.

Name	Fuel Condition	λ	Nominal [NO] undiluted (ppm)	Nominal [NO] diluted (ppm)	H/C	CO	CO_2	NO	N_2	O_2	H_2	He
ch1no50-lean	lean	2.0	50	2	1	0.000430	0.003661	0.000002	0.037622	0.006382	0.001988	0.949915
ch2no50-lean	lean	2.0	50	2	2	0.000344	0.002930	0.000002	0.036561	0.006639	0.003192	0.950332
ch3no50-lean	lean	2.0	50	2	3	0.000286	0.002436	0.000002	0.036007	0.007155	0.004187	0.949926
ch4no50-lean	lean	2.0	50	2	4	0.000252	0.002147	0.000002	0.035507	0.007420	0.004748	0.949923
ch1no500-lean	lean	2.0	500	20	1	0.000430	0.003662	0.000025	0.037281	0.006384	0.001988	0.950229
ch2no500-lean	lean	2.0	500	20	2	0.000344	0.002929	0.000025	0.036591	0.006638	0.003192	0.950281
ch3no500-lean	lean	2.0	500	20	3	0.000286	0.002437	0.000025	0.035814	0.007156	0.004188	0.950094
ch4no500-lean	lean	2.0	500	20	4	0.000252	0.002147	0.000025	0.035463	0.007420	0.004748	0.949944
ch1no5000-lean	lean	2.0	5000	200	1	0.000429	0.003661	0.000255	0.037509	0.006381	0.001987	0.949776
ch2no5000-lean	lean	2.0	5000	200	2	0.000344	0.002929	0.000255	0.036449	0.006638	0.003192	0.950193
ch3no5000-lean	lean	2.0	5000	200	3	0.000286	0.002436	0.000255	0.035895	0.007154	0.004186	0.949787
ch4no5000-lean	lean	2.0	5000	200	4	0.000252	0.002147	0.000255	0.035405	0.007156	0.004749	0.950036
ch1no50000-lean	lean	2.0	50000	2000	1	0.000407	0.003469	0.002500	0.035647	0.005899	0.001988	0.950091
ch2no50000-lean	lean	2.0	50000	2000	2	0.000324	0.002760	0.002499	0.034910	0.006382	0.003191	0.949933
ch3no50000-lean	lean	2.0	50000	2000	3	0.000269	0.002292	0.002500	0.034189	0.006638	0.003915	0.950197
ch4no50000-lean	lean	2.0	50000	2000	4	0.000236	0.002010	0.002500	0.033801	0.006891	0.004461	0.950102
ch1no50-stoi	stoichiometric	0.5	50	2	1	0.000807	0.006883	0.000002	0.036011	0.002361	0.003914	0.950021
ch2no50-stoi	stoichiometric	0.5	50	2	2	0.000641	0.005461	0.000002	0.034509	0.003437	0.005998	0.949952
ch3no50-stoi	stoichiometric	0.5	50	2	3	0.000528	0.004501	0.000002	0.033009	0.004175	0.007843	0.949941
ch4no50-stoi	stoichiometric	0.5	50	2	4	0.000452	0.003854	0.000002	0.032511	0.004568	0.008613	0.949999
ch1no500-stoi	stoichiometric	0.5	500	20	1	0.000808	0.006884	0.000025	0.035818	0.002361	0.003915	0.950189
ch2no500-stoi	stoichiometric	0.5	500	20	2	0.000641	0.005464	0.000025	0.034018	0.003439	0.006001	0.950412
ch3no500-stoi	stoichiometric	0.5	500	20	3	0.000527	0.004494	0.000025	0.033039	0.004175	0.007843	0.949897
ch4no500-stoi	stoichiometric	0.5	500	20	4	0.000452	0.003856	0.000025	0.032146	0.004570	0.008616	0.950335
ch1no5000-stoi	stoichiometric	0.5	5000	200	1	0.000807	0.006882	0.000255	0.035899	0.002361	0.003914	0.949882
ch2no5000-stoi	stoichiometric	0.5	5000	200	2	0.000641	0.005460	0.000255	0.034397	0.003437	0.005997	0.949813
ch3no5000-stoi	stoichiometric	0.5	5000	200	3	0.000527	0.004496	0.000255	0.032917	0.003989	0.007447	0.950368
ch4no5000-stoi	stoichiometric	0.5	5000	200	4	0.000452	0.003854	0.000255	0.032400	0.004567	0.008612	0.949860
ch1no50000-stoi	stoichiometric	0.5	50000	2000	1	0.000774	0.006597	0.002499	0.034184	0.002223	0.003668	0.950054
ch2no50000-stoi	stoichiometric	0.5	50000	2000	2	0.000608	0.005181	0.002499	0.032712	0.003271	0.005997	0.949733
ch3no50000-stoi	stoichiometric	0.5	50000	2000	3	0.000501	0.004273	0.002499	0.031639	0.003798	0.007443	0.949846
ch4no50000-stoi	stoichiometric	0.5	50000	2000	4	0.000430	0.003662	0.002499	0.030725	0.004372	0.008229	0.950083
ch1no50-rich	rich	0.5	50	2	1	0.012843	0.000000	0.000002	0.029167	0.001619	0.006329	0.950039
ch2no50-rich	rich	0.5	50	2	2	0.009919	0.000000	0.000002	0.027816	0.002499	0.009919	0.949846
ch3no50-rich	rich	0.5	50	2	3	0.008304	0.000000	0.000002	0.026469	0.003106	0.012302	0.949817
ch4no50-rich	rich	0.5	50	2	4	0.006815	0.000000	0.000002	0.025634	0.003438	0.013922	0.950189
ch1no500-rich	rich	0.5	500	20	1	0.012842	0.000000	0.000025	0.029305	0.001507	0.006329	0.949992
ch2no500-rich	rich	0.5	500	20	2	0.009921	0.000000	0.000025	0.027547	0.002500	0.009921	0.950087
ch3no500-rich	rich	0.5	500	20	3	0.008304	0.000000	0.000025	0.026361	0.003106	0.012303	0.949901
ch4no500-rich	rich	0.5	500	20	4	0.007094	0.000000	0.000025	0.025597	0.003437	0.013918	0.949930
ch1no5000-rich	rich	0.5	5000	200	1	0.012456	0.000000	0.000255	0.029515	0.001618	0.006328	0.949828
ch2no5000-rich	rich	0.5	5000	200	2	0.009917	0.000000	0.000255	0.027705	0.002499	0.009917	0.949707
ch3no5000-rich	rich	0.5	5000	200	3	0.007997	0.000000	0.000255	0.026367	0.003107	0.012304	0.949970
ch4no5000-rich	rich	0.5	5000	200	4	0.006814	0.000000	0.000255	0.025523	0.003438	0.013920	0.950050
ch1no50000-rich	rich	0.5	50000	2000	1	0.012073	0.000000	0.002499	0.027990	0.001507	0.005998	0.949933
ch2no50000-rich	rich	0.5	50000	2000	2	0.009573	0.000000	0.002499	0.026258	0.002360	0.009457	0.949853
ch3no50000-rich	rich	0.5	50000	2000	3	0.007685	0.000000	0.002499	0.025201	0.002949	0.011803	0.949864
ch4no50000-rich	rich	0.5	50000	2000	4	0.006543	0.000000	0.002499	0.024473	0.003272	0.013378	0.949835

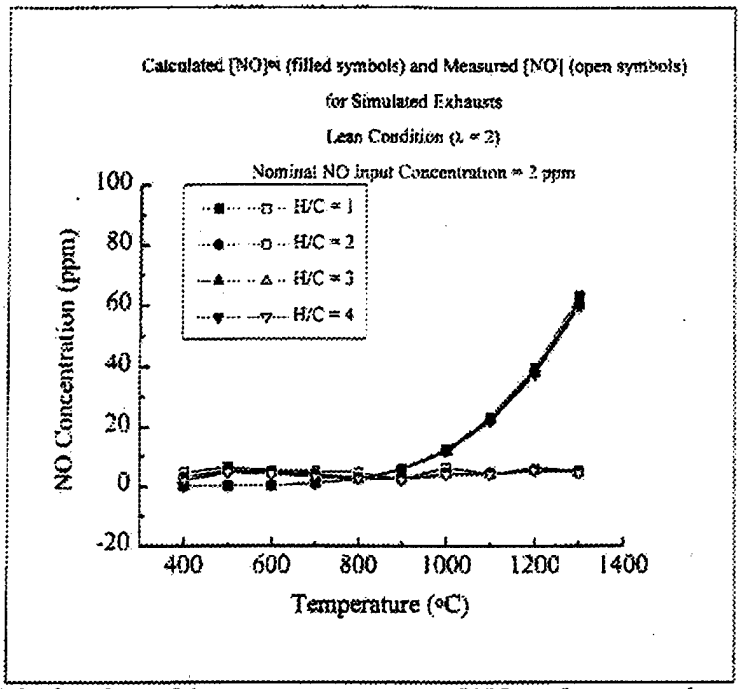

Figure 29: Calculated equilibrium concentration of NO and measured concentration of NO (post-reactor with perovskite catalyst) for all H/C ratios, a fuel-lean condition and a nominal NO input concentration of 2 ppm, as a function of temperature.

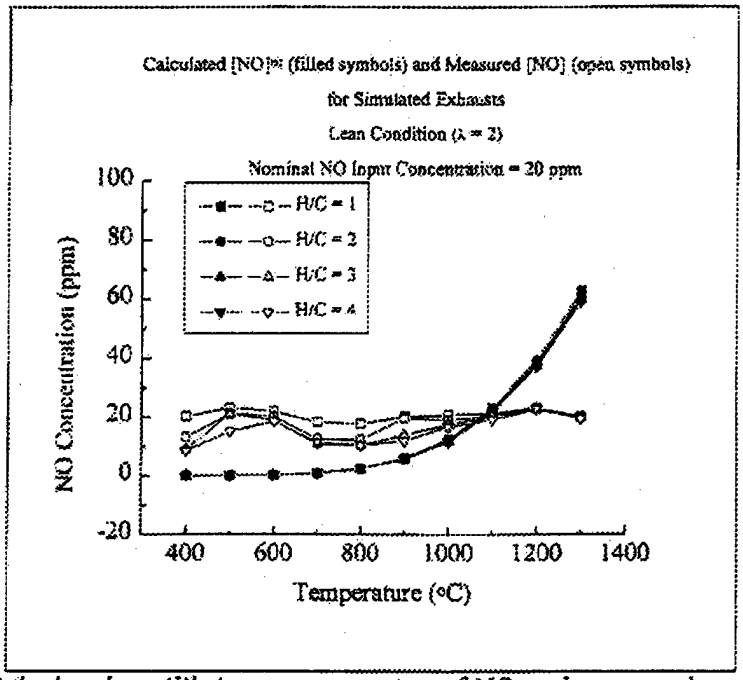

Figure 30: Calculated equilibrium concentration of NO and measured concentration of NO (post-reactor with perovskite catalyst) for all H/C ratios, a fuel-lean condition and a nominal NO input concentration of 20 ppm, as a function of temperature.

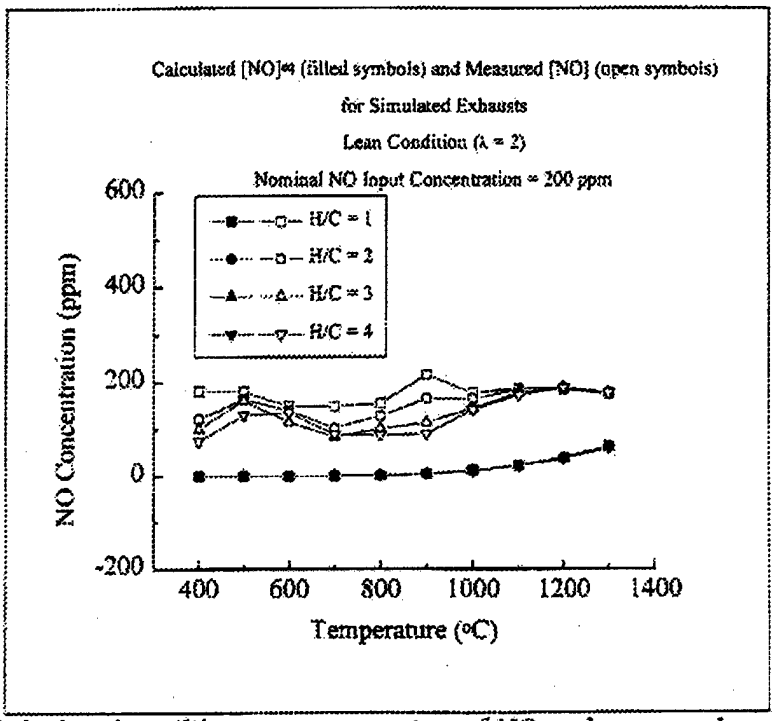

Figure 31: Calculated equilibrium concentration of NO and measured concentration of NO (post-reactor with perovskite catalyst) for all H/C ratios, a fuel-lean condition and a nominal NO input concentration of 200 ppm, as a function of temperature.

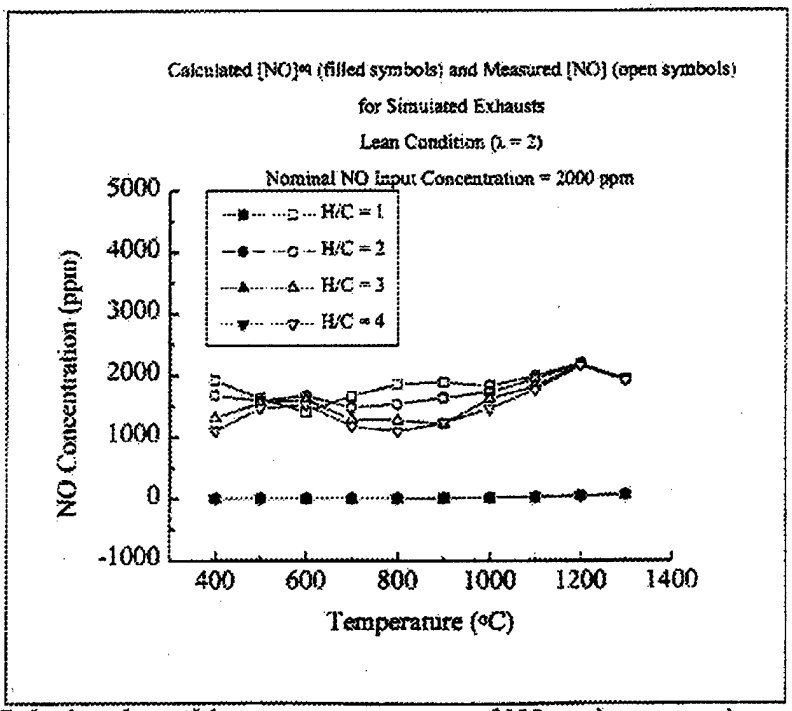

Figure 32: Calculated equilibrium concentration of NO and measured concentration of NO (post-reactor with perovskite catalyst) for all H/C ratios, a fuel-lean condition and a nominal NO input concentration of 2000 ppm, as a function of temperature.

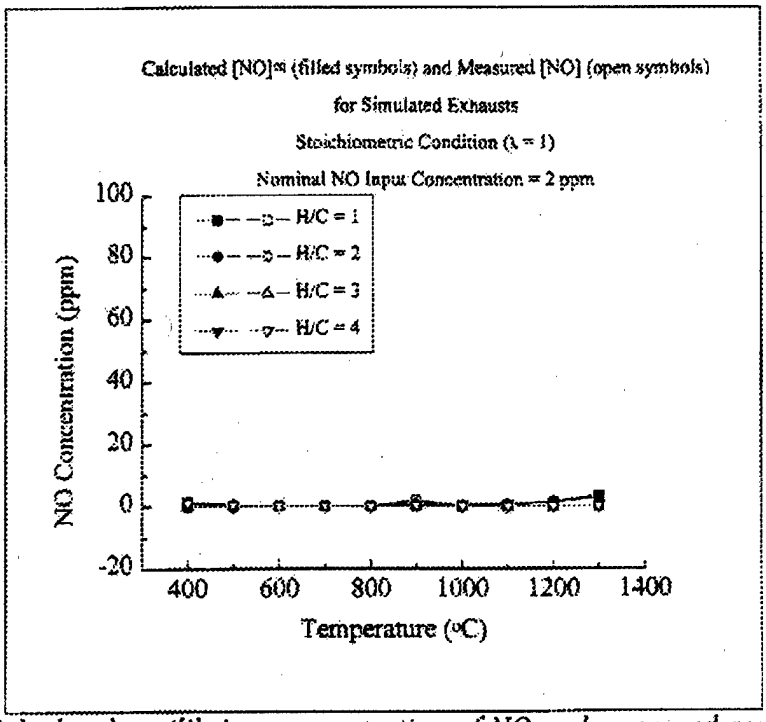

Figure 33: Calculated equilibrium concentration of NO and measured concentration of NO (post-reactor with perovskite catalyst) for all H/C ratios, a stoichiometric condition and a nominal NO input concentration of 2 ppm, as a function of temperature.

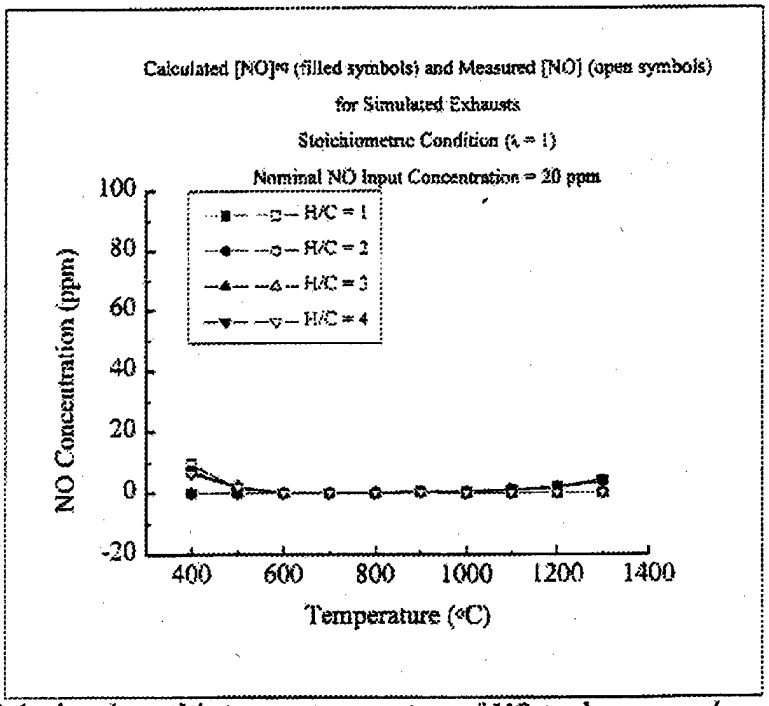

Figure 34: Calculated equilibrium concentration of NO and measured concentration of NO (post-reactor with perovskite catalyst) for all H/C ratios, a stoichiometric condition and a nominal NO input concentration of 20 ppm, as a function of temperature.

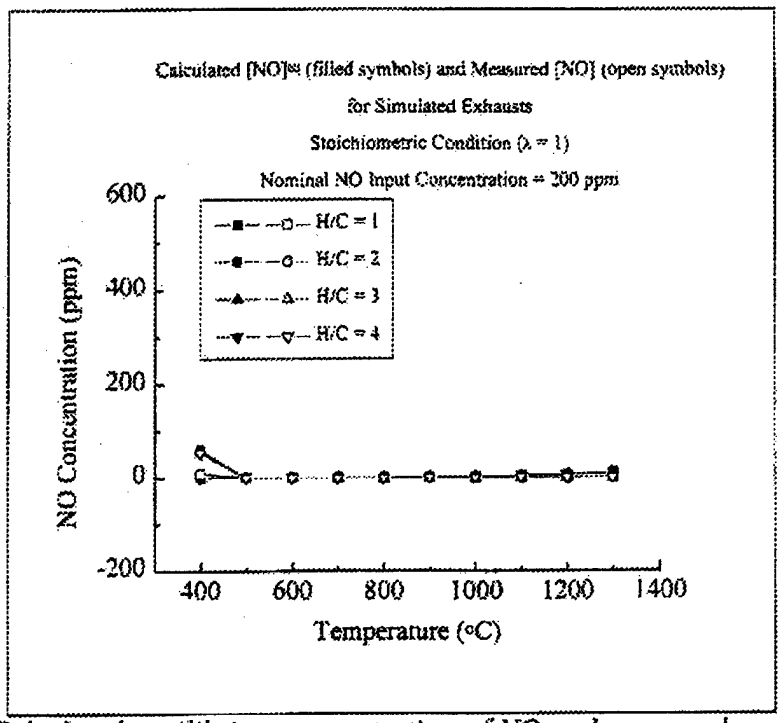

Figure 35: Calculated equilibrium concentration of NO and measured concentration of NO (post-reactor with perovskite catalyst) for all H/C ratios, a stoichiometric condition and a nominal NO input concentration of 200 ppm, as a function of temperature.

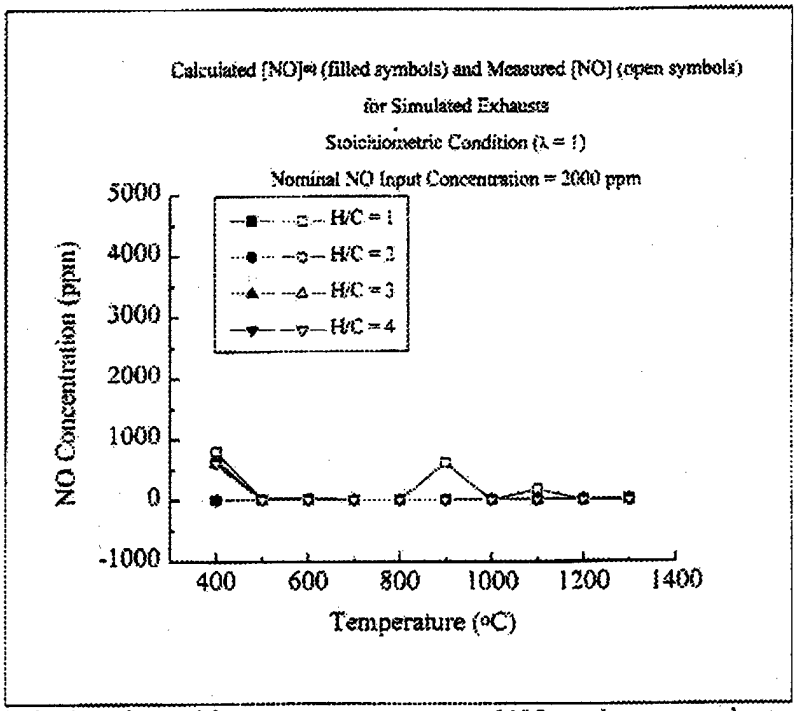

Figure 36: Calculated equilibrium concentration of NO and measured concentration of NO (post-reactor with perovskite catalyst) for all H/C ratios, a stoichiometric condition and a nominal NO input concentration of 2000 ppm, as a function of temperature.

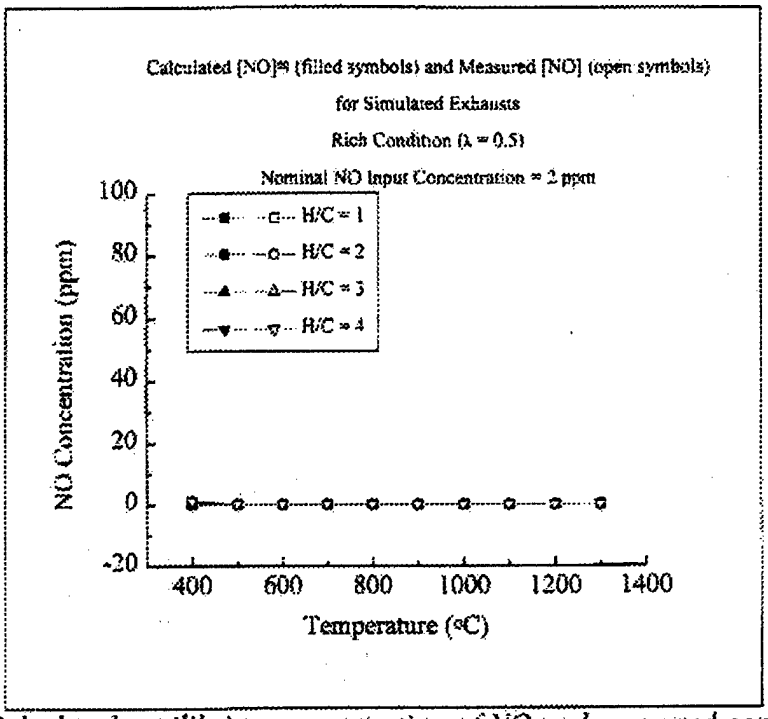

Figure 37: Calculated equilibrium concentration of NO and measured concentration of NO (post-reactor with perovskite catalyst) for all H/C ratios, a fuel-rich condition and a nominal NO input concentration of 2 ppm, as a function of temperature.

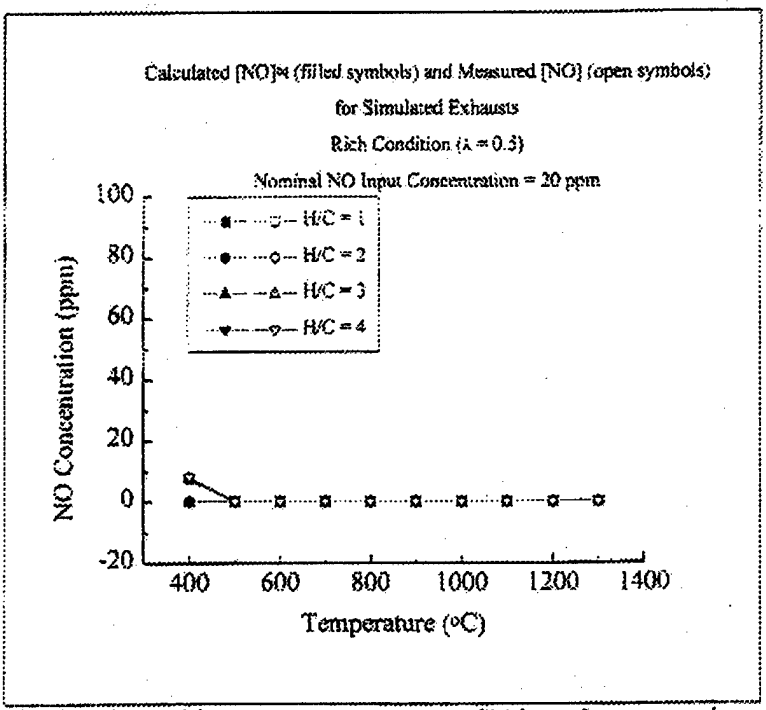

Figure 38: Calculated equilibrium concentration of NO and measured concentration of NO (post-reactor with perovskite catalyst) for all H/C ratios, a fuel-rich condition and a nominal NO input concentration of 20 ppm, as a function of temperature.

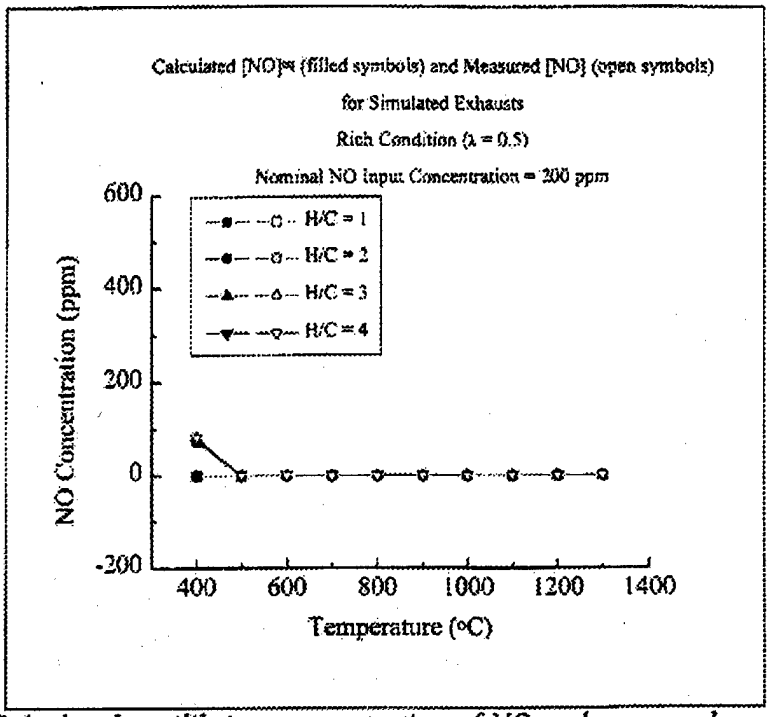

Figure 39: Calculated equilibrium concentration of NO and measured concentration of NO (post-reactor with perovskite catalyst) for all H/C ratios, a fuel-rich condition and a nominal NO input concentration of 200 ppm, as a function of temperature.

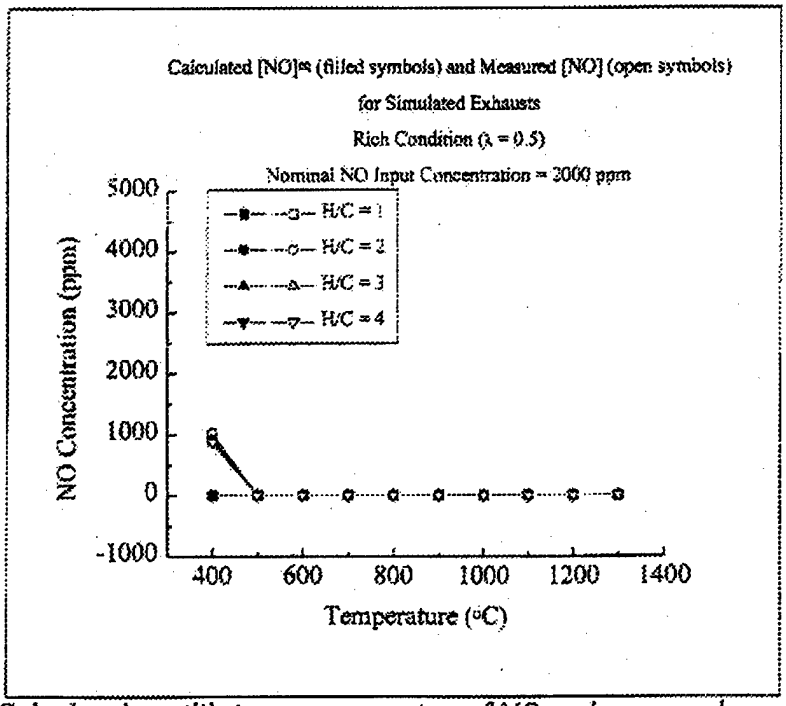

Figure 40: Calculated equilibrium concentration of NO and measured concentration of NO (post-reactor with perovskite catalyst) for all H/C ratios, a fuel-rich condition and a nominal NO input concentration of 2000 ppm, as a function of temperature.

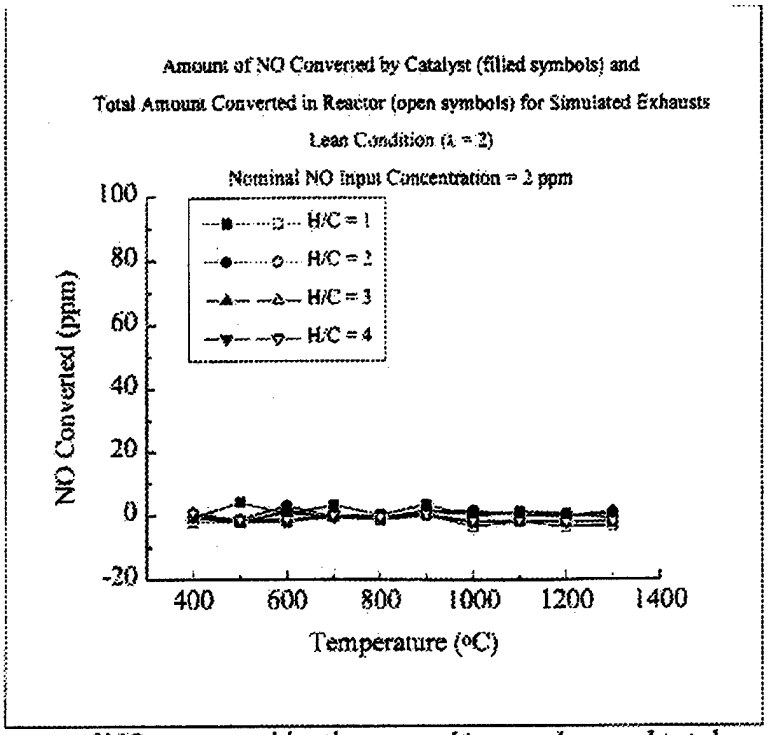

Figure 41: Amount of NO converted by the perovskite catalyst and total amount converted in the annular reactor for all H/C ratios, a fuel-lean condition, and a nominal NO input concentration of 2 ppm as a function of reactor temperature.

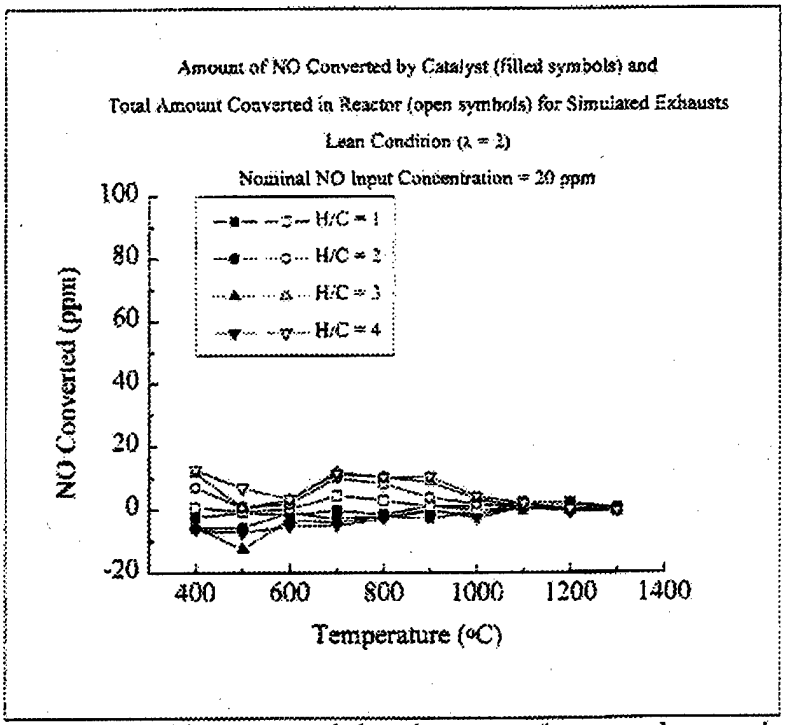

Figure 42: Amount of NO converted by the perovskite catalyst and total amount converted in the annular reactor for all H/C ratios, a fuel-lean condition, and a nominal NO input concentration of 20 ppm as a function of reactor temperature.

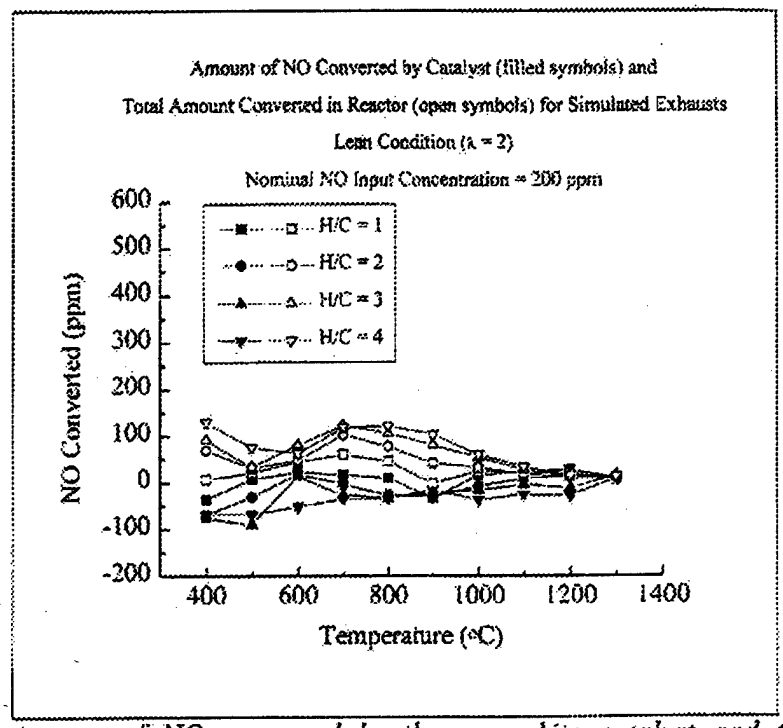

Figure 43: Amount of NO converted by the perovskite catalyst and total amount converted in the annular reactor for all H/C ratios, a fuel-lean condition, and a nominal NO input concentration of 200 ppm as a function of reactor temperature.

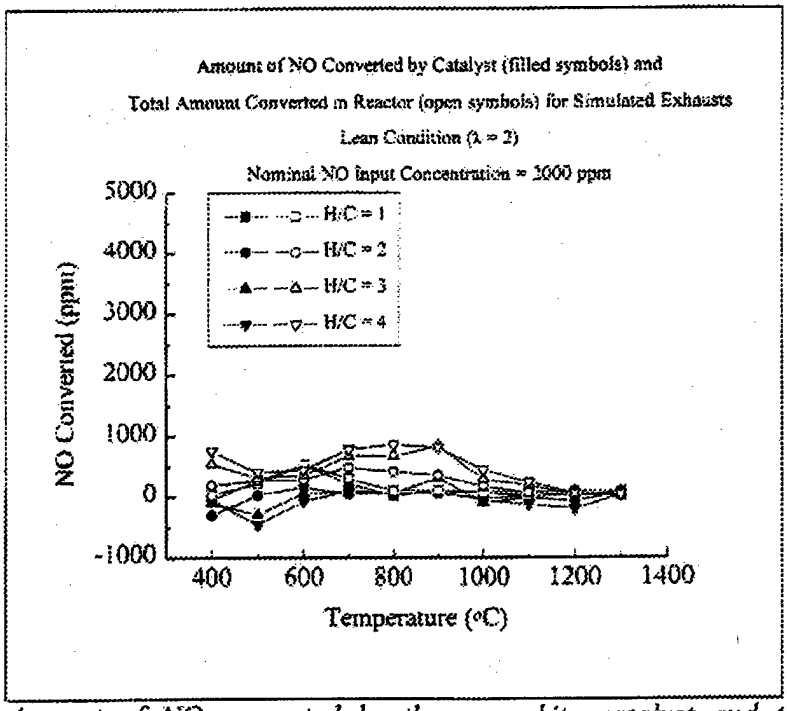

Figure 44: Amount of NO converted by the perovskite catalyst and total amount converted in the annular reactor for all H/C ratios, a fuel-lean condition, and a nominal NO input concentration of 2000 ppm as a function of reactor temperature.

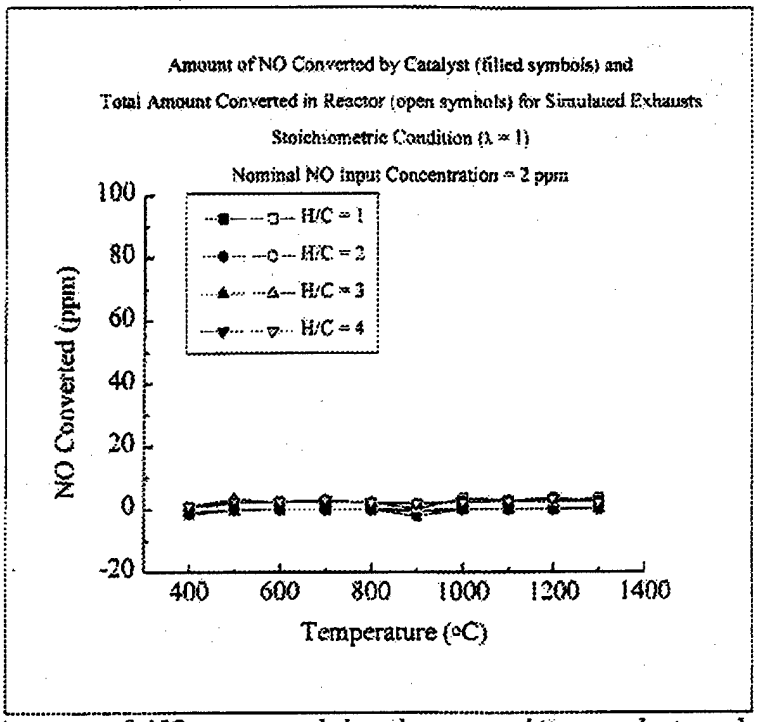

Figure 45: Amount of NO converted by the perovskite catalyst and total amount converted in the annular reactor for all H/C ratios, a stoichiometric condition, and a nominal NO input concentration of 2 ppm as a function of reactor temperature.

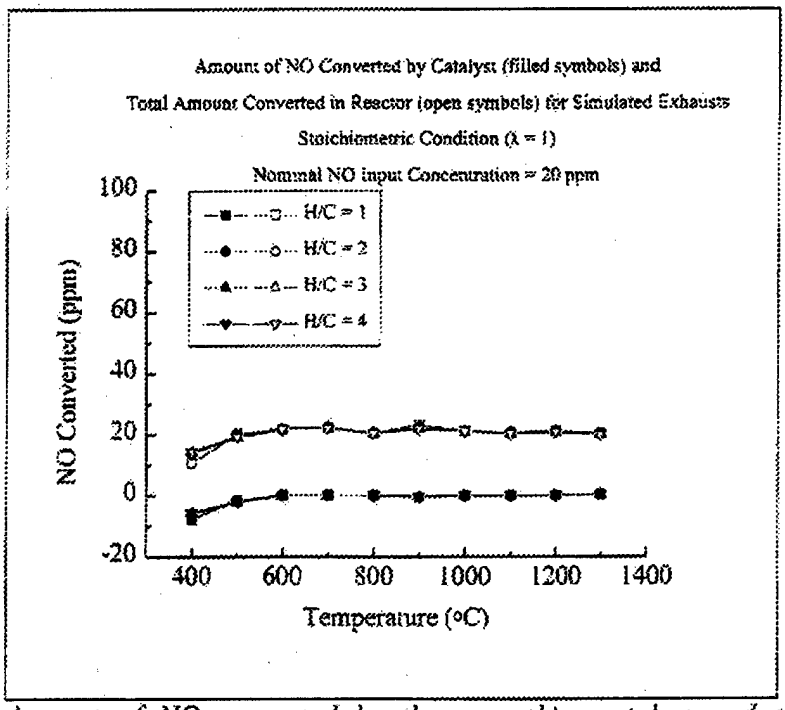

Figure 46: Amount of NO converted by the perovskite catalyst and total amount converted in the annular reactor for all H/C ratios, a stoichiometric condition, and a nominal NO input concentration of 20 ppm as a function of reactor temperature.

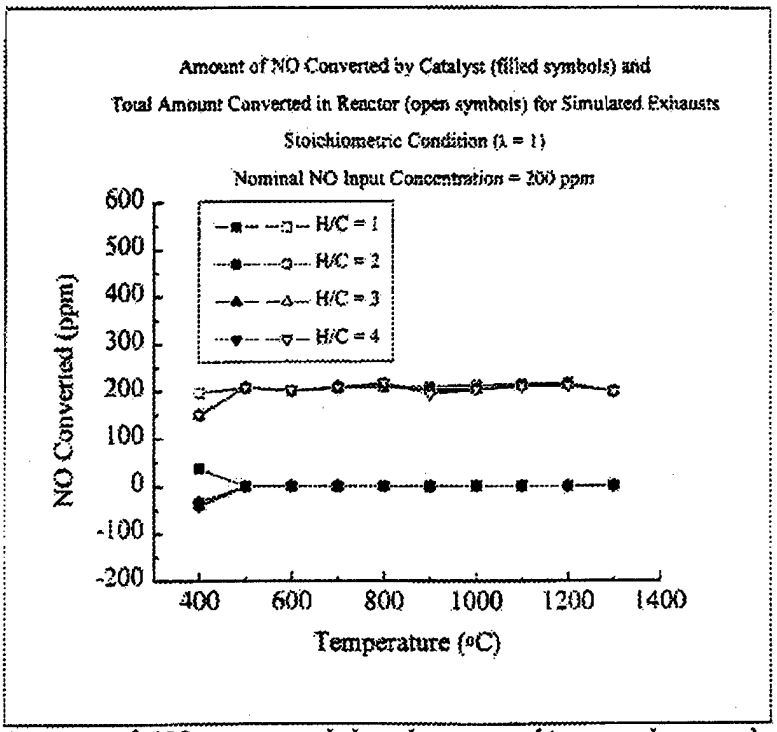

Figure 47: Amount of NO converted by the perovskite catalyst and total amount converted in the annular reactor for all H/C ratios, a stoichiometric condition, and a nominal NO input concentration of 200 ppm as a function of reactor temperature.

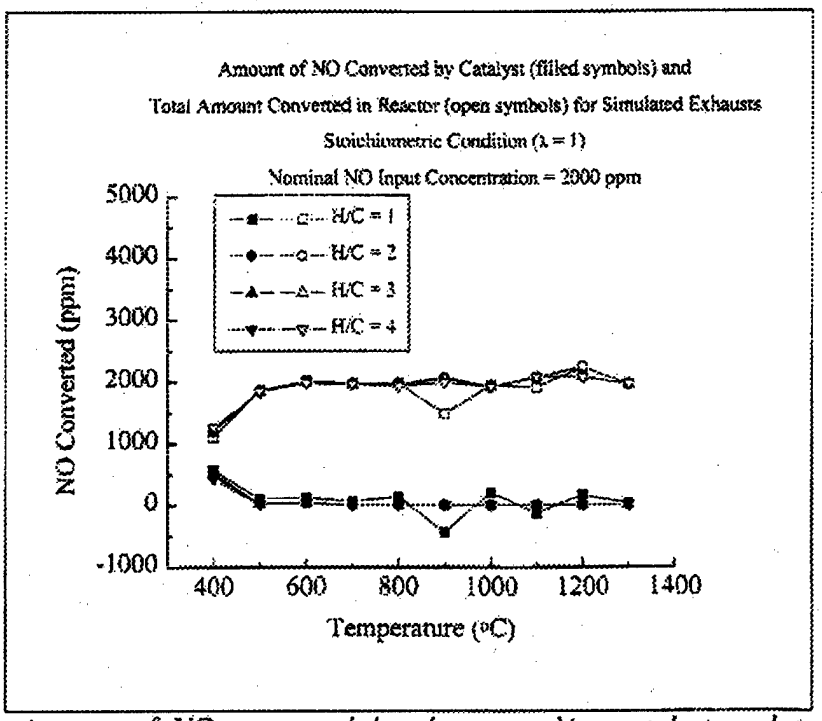

Figure 48: Amount of NO converted by the perovskite catalyst and total amount converted in the annular reactor for all H/C ratios, a stoichiometric condition, and a nominal NO input concentration of 2000 ppm as a function of reactor temperature.

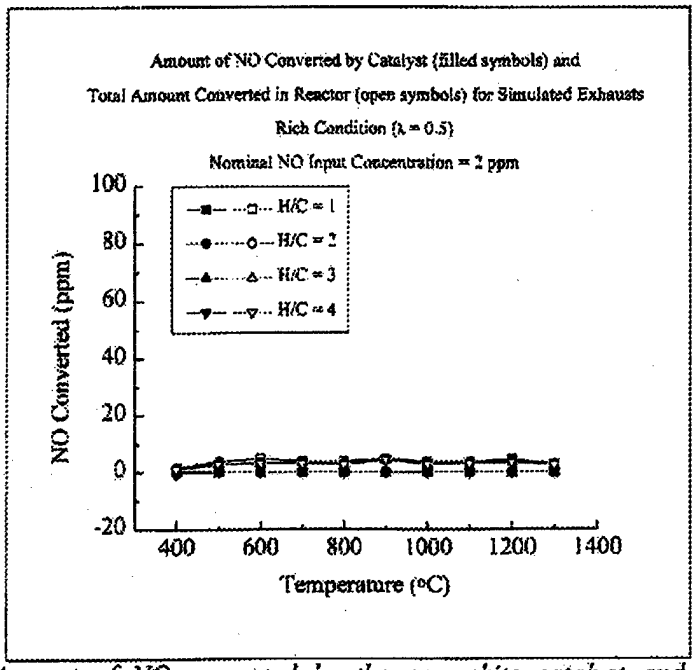

Figure 49: Amount of NO converted by the perovskite catalyst and total amount converted in the annular reactor for all H/C ratios, a fuel-rich condition, and a nominal NO input concentration of 2 ppm as a function of reactor temperature.

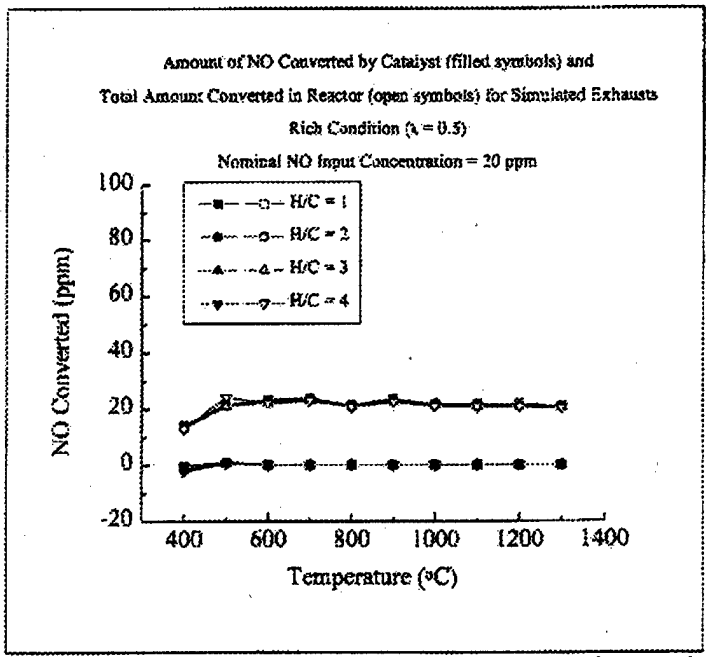

Figure 50: Amount of NO converted by the perovskite catalyst and total amount converted in the annular reactor for all H/C ratios, a fuel-rich condition, and a nominal NO input concentration of 20 ppm as a function of reactor temperature.

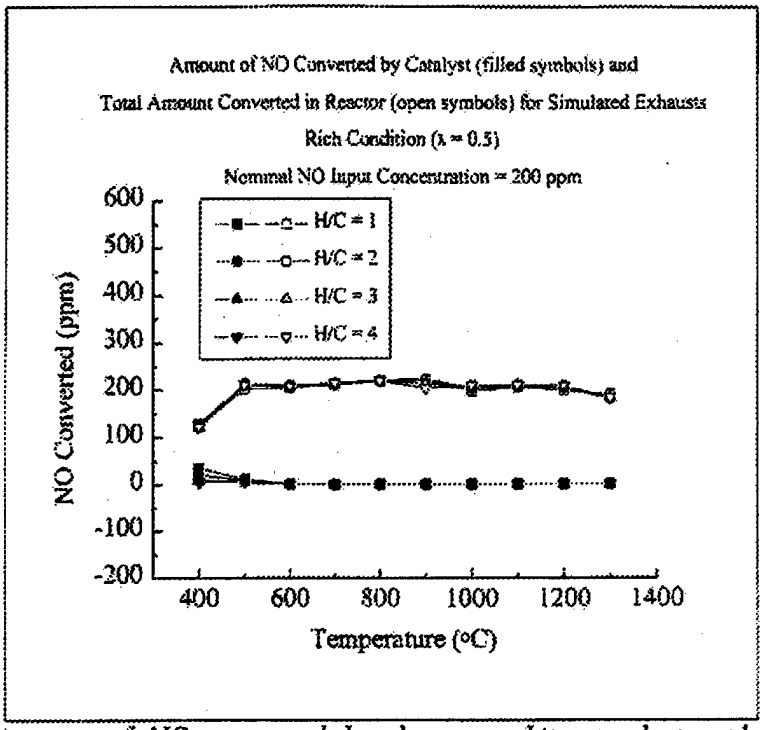

Figure 51: Amount of NO converted by the perovskite catalyst and total amount converted in the annular reactor for all H/C ratios, a fuel-rich condition, and a nominal NO input concentration of 200 ppm as a function of reactor temperature.

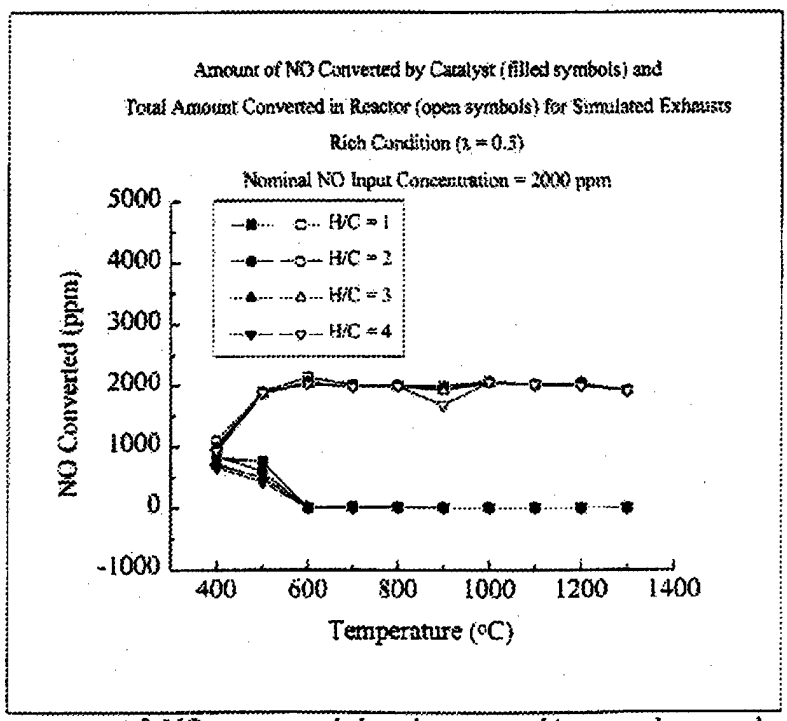

Figure 52: Amount of NO converted by the perovskite catalyst and total amount converted in the annular reactor for all H/C ratios, a fuel-rich condition, and a nominal NO input concentration of 2000 ppm as a function of reactor temperature.

Conclusions and Recommendations

From XRD, DTA and simultaneous TGA/DSC measurements the A-site deficient composition $(La_{0.7}Sr_{0.3})_{0.9}CoO_{2.715}$ was found to be chemically and structurally stable over a wide range of temperatures in air and simulated exhausts. This material will catalyze the reduction of NO to N_2 in the presence of CO under fuel-lean, stoichiometric and fuel rich conditions, and is particularly effective at low temperature. However, the design of any system to do this will be critical because it appears that the kinetic limitations of the reactions would obviate the need for increased contact time between the reactant gases and the catalyst, especially in the lower temperature regime. In addition, the zirconia and alumina materials from which the reactor was constructed definitely appear to enhance the reduction of nitric oxide to nitrogen in the presence of carbon monoxide. Combining substrate materials which seem to enhance NO reduction at high temperatures with the perovskite catalyst, which works best at lower temperatures, holds promise as a synergistic emission control system.

There is still much to be done to assess the real promise of the catalyst. Its effectiveness in reducing the NO_x in simulated high velocity, direct bombardment exhaust gases has not yet been demonstrated. Also, the limits of stability in gases of fluctuating composition, and even the degree of normal fluctuation it would experience in exhaust gases, are not known. One promising enhancement would be a "smart" catalyst/substrate system, capable of protecting itself from deleterious reactions with the environment, utilizing electrochemical feedback to set the emf across the zirconia substrate, thus controlling the oxygen potential experienced by the catalyst.

References

1 W. F. Libby, "Promising Catalyst for Auto Exhaust," Science, 171 [3970] 499-50(1970).

2 D. B. Meadowcroft, "Low-Cost Oxygen Electrode Material," Nature (London), 226 [5248] 847-48 (1970).

3 S. C. Sorensen, J. A. Wronkiewicz, L. B. Sis and G. P. Wirtz, "Properties of $LaCoO_3$ as a Catalyst in Engine Exhaust Gases," Amer. Ceram. Soc. Bull., 53 [5] 446-49 (1974).

4 Voorhoeve, R.J.H., Remeika, J.P., Trimble, L.E., "Nitric oxide and perovskite catalysts: Solid state and catalytic chemistry," The Catalytic Chemistry of Nitrocen Oxides, R.L. Klimisch and J.G. Larson (eds.), Plenum Press, N.Y., pp. 215 (1976).

5 R. J. H. Voorhoeve, D. W. Johnson, Jr., J. P. Remeika, and P. K. Gallagher, "Perovskite Oxides: Materials Science in Catalysis," Science, 14, 395-406 (1975).

6 R. J. H. Voorhoeve, J. P. Remeika, L. E. Trimble, A. S. Cooper, F. J. Disalvo, P. K. Gallagher, "Perovskite-Like $La_{1-x}K_xMnO_3$ and Related Compounds: Solid State Chemistry and the Catalysis of the Reduction of NO by CO and H'," J. Solid State Chem., 14, 395-406 (1975).

7 T. Nakamura, M. Misono, Y. Yoneda, "Reduction-Oxidation and Catalytic Properties of $La_{1-x}Sr_xCoO_3$", J. Catal., 83, 151-59 (1983).

8 M. A. Pena, J. M. D. Tascon, L. G. Tejuca, "Surface Interactions of NO with $LaFeO_3$," Nouv. J. Chim., 9 [10] 591-95 (1985).

9 J. M. D. Tascon, L. G. Tejuca, C. H. Rochester, "Surface Interactions of NO and CO with $LaMO_3$," J. Catal., 95, 558-66 (1985).

10 M. A. Pena, J. M. D. Tascon, J. L. G. Fierro, L. G. Tejuca, "A Study of NO and CO Interactions with $LaMnO_3$," J. Colloid Int. Sci., 119 [1] 100-07 (1987).

11 Properties and Applications of Perovskite-Type Oxides, L. G. Tejuca and J. L. G. Fierro, Ed., Marcel Dekker, Inc. New York (1993).

12 C. S. Tedmon, H. S. Spacil and S. P. Mitoff, J. Electrochem. Soc., 116 [9] 1170 (1969).

13 I. Kojima, H. Adachi, I. Yasumori, "Electronic Structures of the LaBO3 (B=Co, Fe, Al) Perovskite Oxides Related to Their Catalysis," Surface Sci., 130, 50-62 (1983).

[14] M. R. Balasubramanian, R. Natesan, P. Rajendran, "Correlation Between Catalytic Activities and Physicochemical Properties of Perovskite Oxides," J. Sci. Ind. Res., 43, 500-06 (1984).

[15] N. Yamazoe, Y. Teraoka, T. Seiyama, "TPD and XPS Study on Thermal Behavior of Adsorbed Oxygen in $La_{1-x}Sr_xCoO_3$," Chem. Lett., 1767-70 (1981).

[16] Y. Teraoka, M. Yoshimatsu, N. Yamazoe, T. Seiyama, "Oxygen-Sorptive Properties and Defect Structure of Perovskite-Type Oxides," Chem. Lett., 893-96 (1984).

[17] G. P. Wirtz and H. S. Isaacs, "Indium Oxide Electrodes on Stabilized Zirconia Electrolytes," J. Solid State Ionics, 9 [10] 963-72 (1983).

[18] G. P. Wirtz and H. S. Isaacs, "Defect Electrochemistry of Oxide Electrodes," Proceedings of Brookhaven Conference on High Temperature Solid Oxide Electrolytes, BNL-51728, 298-317 (1983).

[19] G. P. Wirtz, "Oxide Electrodes on Yttria Stabilized Zirconia Electrolytes at High Temperatures," Proceedings of the DOE Physical and Chemical Energy Storage Annual Contractors' Review Meeting, U. S. Department of Energy, Conf-830974, 106-11 (1983).

[20] G. Reinhardt, V. Baitinger, W. Goepel, "Oxygen Electrodes of Zirconia Electrolytes: Fundamentals and Applications to the Analysis of Oxygen Containing Gases," Proceedings of the 2nd Euroconference on Solid State Ionics, to be published (1995).

[21] J. C. C. Abrantes, F. M. B. Marques and J. R. Frade, "Electrical Conductivity of La_{1-x},MnO_{3-y} Perovskites," Proc. 2nd European Cer. Soc. Conf., Augsburg (1991).

[22] J. Mizusaki, Y. Mima, S. Yamauchi, K. Fueki and H. Tagawa, "Nonstoichiometry of the Perovskite-Type Oxides $La_{1-x}Sr_xCoO_{3-}$, " J. Sol. State Chem., 80, 102-111 (1989).

[23] T. Nakamura, G. Petzow and L. J. Gauckler, "Stability of the Perovskite Phase $LaBO_3$ (B = V, Mn, Fe, Co, Ni) in Reducing Atmospheres," Mat. Res. Bull., 14, 649-659 (1979).

[24] M. Boudart, "Kinetics in Catalysis", in Perspectives in Catalysis, International Union or Pure and Applied Chemistry, London (1992) p. 183.

[25] T. Nakamura, M. Misono, and Y. Yoneda, "Catalytic Properties of Perovskite-type Mixed Oxides, $La_{1-x}Sr_xCoO_3$," Bull. Chem. Soc. Jpn., 55 [2] 394-399 (1982).

[26] B. Viswanathan and S. George, "On the Nature of Active Species in the Oxidation of CO on $LnCoO_3$ Type Perovskites," Indian Journal of Technology, 23, 470-472 (1985).

[27] M. Boudart and G. Djéga-Mariadassou, Kinetics of Heterogeneous Reactions, Princeton University Press, Princeton, NJ (1984) p. 105.